

# Generating, Fast and Slow: Scalable Parallel Video Generation with Video Interface Networks

Bhishma Dedhia<sup>1,2,\*</sup>, David Bourgin<sup>2</sup>, Krishna Kumar Singh<sup>2</sup>, Yuheng Li<sup>2</sup>,  
Yan Kang<sup>2</sup>, Zhan Xu<sup>2</sup>, Niraj K. Jha<sup>1</sup>, Yuchen Liu<sup>2,†</sup>  
<sup>1</sup> Princeton University, <sup>2</sup> Adobe Research

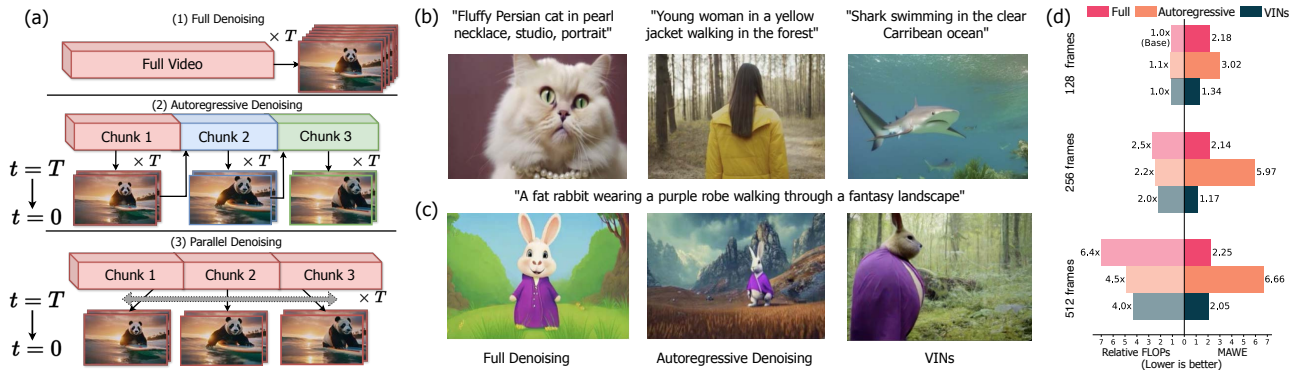


Figure 1. (a) Concept: Video generation has traditionally proceeded with the computationally expensive full generation or the autoregressive alternative that requires repeated inference through a sampling chain. Instead, we formulate a parallel inference paradigm: Video Interface Networks (VINs). (b) VINs enable the generation of long dynamic realistic videos that (c) often stagnate in the full attention setting or lose temporal coherence in the autoregressive setting. (d) Our method uses fewer FLOPs and achieves greater temporal consistency as captured by the Motion Aware Warped Error [17].

## Abstract

Diffusion Transformers (DiTs) can generate short photo-realistic videos, yet directly training and sampling longer videos with full attention across the video remains computationally challenging. Alternative methods break long videos down into sequential generation of short video segments, requiring multiple sampling chain iterations and specialized consistency modules. To overcome these challenges, we introduce a new paradigm called Video Interface Networks (VINs), which augment DiTs with an abstraction module to enable parallel inference of video chunks. At each diffusion step, VINs encode global semantics from the noisy input of local chunks and the encoded representations, in turn, guide DiTs in denoising chunks in parallel. The coupling of VIN and DiT is learned end-to-end on the denoising objective. Further, the VIN architecture maintains fixed-size encoding tokens that encode the input via a single cross-attention step. Disentangling the encoding tokens from the input thus enables VIN to scale to long videos and learn essential semantics. Experiments on VBench demonstrate that VINs

surpass existing chunk-based methods in preserving background consistency and subject coherence. We then show via an optical flow analysis that our approach attains state-of-the-art motion smoothness while using 25-40% fewer FLOPs than full generation. Finally, human raters favorably assessed the overall video quality and temporal consistency of our method in a user study. All videos shown in this manuscript can be found [here](#).

## 1. Introduction

Diffusion Transformers (DiTs) [34] have heralded a revolution in generative modeling and have been scaled up to generate images [5], videos [3, 9, 44, 54], and 3D assets [31] at unprecedented fidelity. Training DiTs on longer input contexts yields remarkable generalization, albeit imposing quadratic computational and memory bottlenecks. The implications are particularly apparent in the case of high-dimensional modalities like video, where training and inference with DiTs on long videos ( $> 64$  frames) are slow and expensive [9] (see Fig 1(a), Full Denoising). Further-

\*Work partially done during an internship at Adobe

† Corresponding Author {yuliu@adobe.com}

more, base models trained on short videos often show motion stagnation and repetition when extended to synthesize longer videos [2, 17]. Practitioners circumvent these constraints by generating video frames in temporal chunks using the previously generated frames as a context window for the next chunk [1, 19] proceeding in a left-to-right sequence (Fig. 1(a), Autoregressive Denoising)

Generating videos sequentially is challenging because, at any given instance, the model only has a finite context. As a result, it may be susceptible to catastrophic forgetting and fail to preserve object coherence and temporal consistency in output generation. Past works [6, 17, 50] have improved the robustness of autoregression by augmenting it with long-term memory modules and image embeddings to enforce semantic and content continuity. Most techniques rely on handpicked anchors and it is not evident that a static prior suffices for generating dynamic videos. *Is sequential generation the only viable approach to generating video chunks? If not, can we devise an alternative paradigm?*

We draw inspiration from accounts of human cognition [12, 22, 42] that suggest that human planning adaptively switches between dual modes of ‘fast’ and ‘slow’ thinking: (1) fast effortless System 1 processing that quickly abstracts out the essence without focusing on the specifics, and (2) slow effortful System 2 processing that uses the intuited semantics to deliberate over finer details. Consider how painters approach their work – they begin by conceptualizing the overall composition through a rough sketch (System 1) before filling in colors for different objects (System 2). This natural parallelization of abstraction and generation (Fig 1(a), Parallel Denoising) remains elusive to DiTs, which solely rely on System 2-like sequential generation of low-level patches, lacking System 1 abstractions.

In this work, we introduce a video-generation paradigm that explicitly augments DiTs with a System 1-like module we call Video Interface Networks (VINs). The central insight behind VINs is simple – at each diffusion timestep, VINs encode meaningful semantics from noisy input videos into a finite set of global tokens that enable scaling to longer videos. Then, the coarse-grained global tokens guide DiTs in denoising fine-grained local tokens of disparate video chunks. The interplay of System 1 via VINs and System 2 via DiTs enables efficient parallel generation of long photorealistic videos (see Fig. 1(b)). Unlike full attention settings that diminish motion and sequential generation that obscures temporal coherence, VINs preserve both the crucial elements (Fig. 1(c)). Prior works on parallelizing video generation models use pre-specified templates, like noise rescheduling [37] or band-pass filtering [29], to enforce consistency. Instead, we train our proposed framework end-to-end, which naturally yields consistency via emergent global tokens. Our core contributions are as follows.

- We develop a hierarchical learning paradigm that com-

bins *abstraction* with *generation* to enable parallel generation of temporally consistent video chunks. We propose the VIN architecture (Section 3.2) to encode essential semantics of long videos. We then formulate a training objective (Section 3.3) to tightly couple the abstraction abilities of VINs with the generative abilities of DiTs and scale the joint architecture to long videos.

- We evaluate our framework against other state-of-the-art autoregressive and parallel chunk-generation techniques [1, 17, 29, 37]. Experiments on VBench [20] (Section 4.3) demonstrate that VINs best preserve subject/background consistency across chunks and reduce the performance gap to computationally-expensive full generation. Optical flow analysis (Section 4.4) shows VINs enable pixel-level motion smoothness. VINs not only attain state-of-the-art Motion Aware Warp Error (MAWE) scores but also exhibit a superior consistency-dynamic degree tradeoff compared to the full generation at different video lengths.
- We conduct a user study (Section 4.6) that bridges the subjectivity gap between our analysis and human ratings, demonstrating the human preference for VIN-generated videos across overall appearance and temporal consistency evaluations.

## 2. Related Work

**Diffusion Architectures for Videos.** Latent Diffusion models [18, 19, 40, 43] have become the predominant approach for generating videos from text or image prompts. Early works [1, 2, 8, 14, 16, 47] focused on temporally extending pre-trained models by interleaving temporal attention with spatial attention. Subsequently, at the outset of DiTs [34], these modeling choices were simplified to denoise a sequence of video patches using Transformers [3, 9, 15, 30, 44] and yielded an unprecedented level of generalization. Training of longer sequence Transformer models can be enabled by parallelization techniques [26, 39, 41, 53], but they require massive computational resources and hardware-aware optimization. In contrast, our VIN amortizes the scaling cost into encoding global tokens.

**Autoregressive Video Generation.** Base models [1, 14] trained on short videos noticeably deteriorate when extended to longer videos. An important line of work [1, 6, 17, 19, 32, 50] has therefore focused on autoregressively generating temporal chunks of long videos. Sequential generation is slow, requiring each video chunk to be denoised over multiple sampling steps. Moreover, to mitigate forgetting, these methods need conditioning for global consistency, such as long-term memory modules [17], image embeddings [6, 48, 50, 52] or specialized priming [13, 51]. Pre-specified anchors increase controllability but limit the content and dynamics, are unscalable, and need specialized encoding architectures. In contrast, VINs maintain dynamic

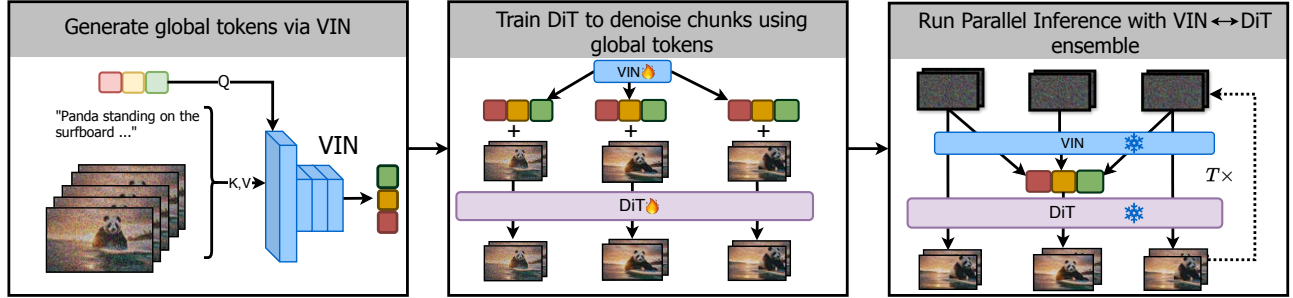


Figure 2. Overview of our method. At each diffusion timestep, the noisy sample is encoded by the VIN to generate global tokens (left, Section 3.2). The VIN is trained end-to-end with the DiT by learning to denoise temporal chunks of the noisy input using the global tokens (middle, Section 3.3). At inference time, The VIN-DiT ensemble can run parallel inference on long videos (right, Section 3.4).

global priors and can be scaled to entire video.

**Parallel Video Generation.** Orthogonal to autoregressive generation, recent works [28, 29, 37, 46] have proposed generating video chunks in parallel. The central challenge lies in designing global priors that enforce inter-chunk consistency. VideoDrafter [28] generates distinct image priors for each chunk, causing temporal inconsistency. Training-free methods like FreeNoise [37] and FreeLong [29] introduce consistency priors through a noisy input and frequency filtering, respectively. Still, such priors primarily operate on surface-level visual features and fail to capture higher-level semantic abstractions. Our VINs explicitly learn deep features for global semantics at every diffusion timestep.

**Learning to Abstract for Generation.** Multiple approaches [21, 35, 36] integrate learning semantic encoders with the denoising objective to guide the diffusion process. Our approach is inspired by Recurrent Interface Networks (RINs) [21] that offload pixel-level denoising to learned semantic tokens. VINs combine the scalability of RIN-like architectures with DiTs. Another approach [35] trains an encoder concurrently with the denoiser to produce semantic codes for efficient diffusion but is limited to images.

### 3. Methodology

Our overall goal (see Fig. 2) is to (1) encode long videos into a finite set of global tokens, (2) train DiTs to generate short video chunks using the encoded tokens, and (3) combine the architectures to run parallel inference.

#### 3.1. Preliminaries

**Diffusion Models** learn to generate data by reversing a gradual noising process over  $T$  timesteps. The central learning objective involves learning a neural network  $\epsilon_\theta(x_t, t)$  to predict noise  $\epsilon_t$  from noisy input  $x_t$ . The model  $\epsilon_\theta(x_t, t)$  is trained via the following regression loss:

$$\mathcal{L}_\theta = \mathbb{E}_{t \sim \mathcal{U}(0, T), \epsilon_t \sim \mathcal{N}(0, 1)} \left[ \|\epsilon_\theta(x_t, t) - \epsilon_t\|^2 \right]. \quad (1)$$

**Diffusion Transformers** model noisy input videos as a sequence of space-time patches. For a noisy video  $x \in \mathbb{R}^{H \times W \times F \times C}$ , let us denote  $H$  as height,  $W$  as width,

$F$  as frames, and  $C$  as input channels. Disjoint voxels of size  $(p_1, p_2, p_3)$  are projected onto  $N$  tokens  $X^{1:N} \in \mathbb{R}^{H/p_1 \times W/p_2 \times F/p_3 \times d}$  by a feedforward network  $G_\theta(\cdot)$ . At denoising time-step  $t$ , the DiT passes the sequence of tokens with the text prompt embedding  $T_{emb}$  through a stack of  $L$  standard transformer blocks  $\mathcal{T}_\theta^{1:L}$ :

$$X_t^{1:N, l} = \mathcal{T}_\theta^l \left( \left[ X_t^{1:N, l-1}, T_{emb} \right], t \right) \forall l \in 1, \dots, L. \quad (2)$$

The final token representations  $X^{1:N, L}$  are projected back to input shape by feedforward network  $H_\theta(\cdot)$  to obtain noise prediction  $\hat{\epsilon}_t$ . DiTs denoise inputs  $x_t$  via quadratic self-attention on input representations, but scaling to longer videos is computationally prohibitive. We circumvent this cost using VINs, whose central computational processing is decoupled from the input.

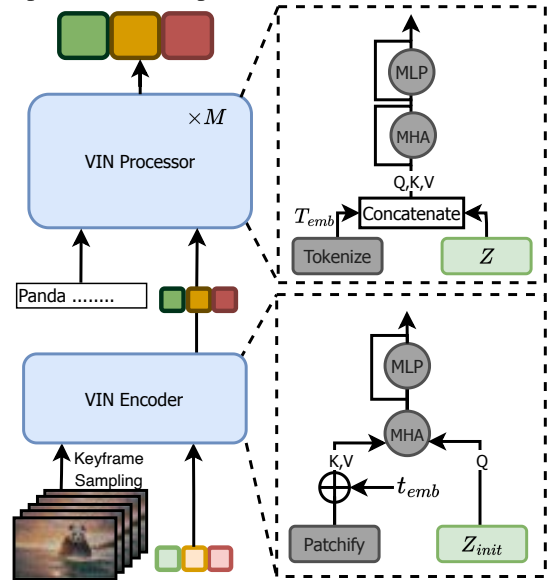


Figure 3. VIN Architecture. The VIN encoder samples key-frames from the input video every  $T_s$  seconds. Then, the global tokens encode the sub-sampled video via cross-attention. A stack of  $M$  VIN Processor blocks refines the global tokens using self-attention.

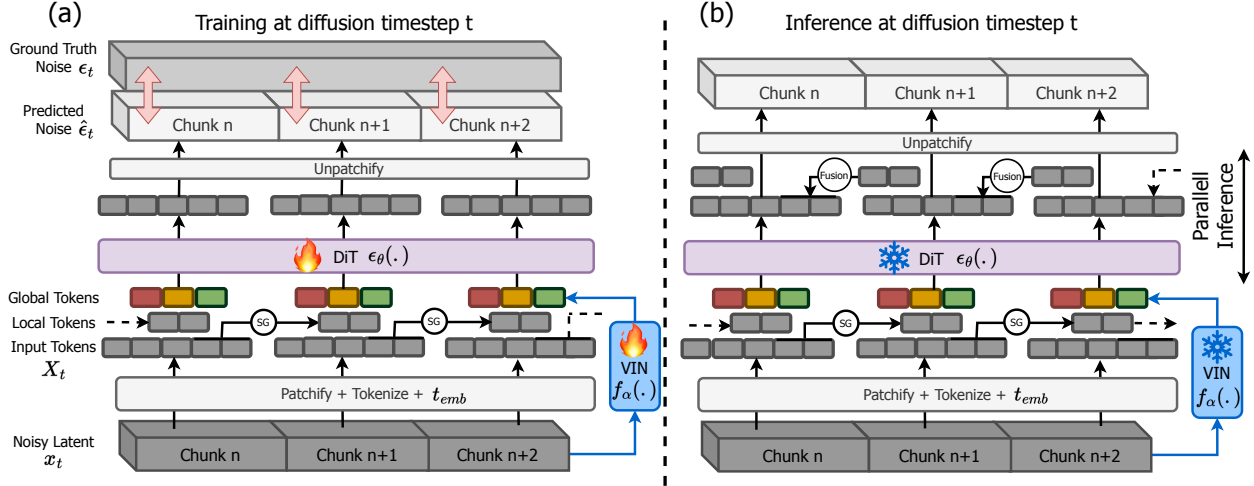


Figure 4. Training and inference configuration. (a) During training, the VIN and DiT are trained end-to-end to denoise video chunks. (b) At inference time, the architectures are frozen to run parallel denoising with token fusion. SG denotes the stop gradient operation.

### 3.2. Video Interface Networks

VINs condense videos with arbitrary lengths into essential semantics (see Fig. 3). VINs encode the inputs into a set of **global tokens** via the **VIN encoder**. Then, VIN models these tokens via consecutive blocks of the **VIN processor**. We describe each of the components in detail next.

**Global Tokens** are at the heart of the VIN backbone. They are instantiated as fixed-sized embeddings  $Z_{init} \in \mathbb{R}^{N_{global} \times d}$ , independent of the input.

**VIN Encoder** encodes the input into the global tokens. First, we sub-sample the input video  $X_t^{1:N}$  at fixed time intervals  $T_s$  to obtain the key-frames  $X_t^{1:N, T_s}$ . Then, the encoder uses the multi-head attention (MHA) mechanism to read the sub-sampled video into  $Z_{init}^{1:N_{global}}$ . More specifically, we derive the query vectors  $Q$  from  $Z_{init}^{1:N_{global}}$  and key-values vectors from  $X_t^{1:N, T_s}$ . The query-key-value interaction enables the selective encoding of the input in the global tokens to obtain input-aware instantiation  $Z_t$ :

$$Z_t = MHA(Q = Z_{init}; K, V = X_t^{1:N, T_s}) \quad (3)$$

**VIN Processor** iteratively refines the instantiated tokens via self-attention. In addition, latents are also conditioned on prompt  $T_{emb}$ :

$$Z_t = MHA(Q, K, V = [Z_t, T_{emb}]) \quad (4)$$

We stack  $M$  blocks together such that the bulk of the VIN computation is allocated to refining the global tokens.

### 3.3. Learning Objective

DiTs and VINs have orthogonal strengths – DiTs excel at modeling fine-grained details in short video segments, while VINs can filter redundancy to learn higher-level features from longer videos. Our strategy is to formulate a

learning objective that couples the complementary abilities of DiTs and VINs to generate long videos. To this end, we first integrate the global tokens in the noise estimate of denoising step  $t$ :

$$P_\theta(\epsilon_t | X_t, t) = \int P_\theta(\epsilon_t | X_t, t, Z_t) P_\alpha(Z_t | X_t, t) dZ \quad (5)$$

Next, we relax and factorize the noise distribution across temporal chunks. Let the video with  $F$  frames have  $N$  tokens. Correspondingly, each chunk with  $F_{chunk}$  frames contains  $N_s$  tokens. The resulting factorization is given by:

$$P_\theta(\epsilon_t | X_t, t, Z_t) = \prod_{i=0}^{\lfloor N/N_s \rfloor} P_\theta(\epsilon_t^{iN_s:(i+1)N_s} | X_t^{iN_s:(i+1)N_s}, t, Z_t) \quad (6)$$

We parametrize  $P_\theta(\cdot)$  as a DiT network  $\epsilon_\theta(\cdot)$  and  $P_\alpha(\cdot)$  as a point estimate from the VIN network  $\delta(f_\alpha(\cdot))$ . The learning objective resulting from the factorized formulation is as follows:

$$Z_t = f_\alpha(X_t, Z_{init}^{1:N_{global}}) \quad (7)$$

$$\mathcal{L}_{\alpha, \theta} = \mathbb{E}_{\epsilon_t \sim \mathcal{N}(0, 1)} \left[ \sum_{i=0}^{\lfloor N/N_s \rfloor} \|\epsilon_\theta([X_t^i, Z_t], t) - \epsilon_t^i\|^2 \right] \quad (8)$$

where  $X_t^i \equiv X_t^{iN_s:(i+1)N_s}$  and  $\epsilon_t^i \equiv \epsilon_t^{iN_s:(i+1)N_s}$  denote the  $i^{th}$  chunk of the input and noise estimate, respectively. Eq. (8) enables the DiT to simultaneously train on different temporal chunks in parallel. Moreover, end-to-end training enables the architectures to bootstrap off each other where (1) the DiT learns to ground denoising in encoded tokens and (2) the VIN learns to refine global tokens to enable downstream denoising. In practice, neighboring chunks have useful local contexts for denoising. During training,

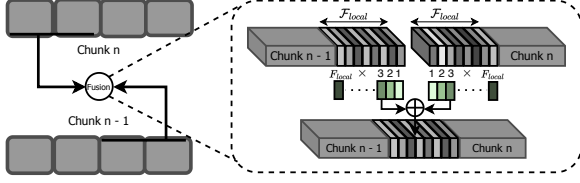


Figure 5. Inference Time Token Fusion. Overlapping tokens in neighboring chunks are combined by a weighted average of their relative temporal position in the chunk.

for each chunk  $i$ , we also append  $N_{local}$  tokens from the last  $F_{local}$  frames of the previous chunk  $i - 1$  to the DiT.

$$\hat{\epsilon}_t^i = \epsilon_\theta \left( [X_t^i, Z_t, SG(X_t^{i-1, N_{local}})], t \right) \quad \forall i \in 0, \dots, \lfloor N/N_s \rfloor \quad (9)$$

Here,  $SG(\cdot)$  stands for the stop gradient operation. We observed that sharing gradients between chunks worsens model output fidelity. Hence, we use  $SG(\cdot)$  to prevent inter-chunk gradient flow. Fig. 4(a) visualizes the training step at diffusion timestep  $t$ .

### 3.4. Inference Method

Inference at time-step  $t$  proceeds by (1) encoding the current estimate  $x_t$  into the global tokens  $Z_t$  via VINs and (2) using  $Z_t$  to denoise chunks parallelly via the DiT to obtain the next sample  $x_{t-1}$ . As outlined in Eq. (9), the adjacent chunks contain overlapping local context and the shared context may diverge across chunks after individual denoising. We mitigate the divergence by fusing the overlapping tokens (see Fig. 5) of noise prediction  $\hat{\epsilon}_t$ . For each position  $k$  in the overlap region between chunks  $\hat{\epsilon}_t^i$  and  $\hat{\epsilon}_t^{i+1}$ , we fuse the overlapping tokens through the following weighted average:

$$\hat{\epsilon}_t^{\text{fused}}[k] = \frac{(\mathcal{F}_{local} - \mathcal{W}(k)) \hat{\epsilon}_t^i[k] + \mathcal{W}(k) \hat{\epsilon}_t^{i+1}[k]}{\mathcal{F}_{local}} \quad (10)$$

Here,  $\mathcal{W}(k) \in \{1, \dots, \mathcal{F}_{local}\}$  denotes the *relative* temporal position of the token in the overlapping region. We also investigate fusion schedules in the sampling chain as follows: (a) early fusion: token fusion applied in initial stages  $t > t_\alpha$ , (b) mid fusion: fusion constrained to specific sampling interval  $t_\alpha < t < t_\beta$ , and (c) late fusion: fusion implemented exclusively in latter steps  $t < t_\alpha$ . Fig. 4(b) visualizes the inference at diffusion timestep  $t$  along with token fusion. Appendix 11 details the joint VIN and DiT training and inference algorithms.

## 4. Experiments

We assess the capability of VINs to generate video chunks with temporal consistency and semantic coherence, benchmarking it against state-of-the-art sequential and parallel generation approaches.

### 4.1. Experimental Setup

**Base Model:** Our method fine-tunes a pre-trained latent video DiT based on a modified Open-Sora variant [54]. The base model encodes 16 video frames into five latent frames using a 3D Variational Auto-Encoder [25]. The final videos are generated at  $192 \times 320$  resolution and 16 FPS.

**VIN:** We augment the base model with the proposed VIN backbone. The architecture uses one encoder and  $M = 4$  processor blocks, modeling  $N_{global} = 512$  tokens with 32 attention heads and hidden dimension  $d = 4096$ . The VIN encoder samples input frames every  $T_s = 1.0s$ .

**Training Dataset:** Our models are trained on 840000 captioned videos. These videos are licensed and have been filtered to remove low-quality content. The training set consists of a mix of  $\{64, 128, 256\}$  frames or  $\{20, 40, 80\}$  latent frame videos.

**Training Details:** The VIN and DiT ensemble are trained end-to-end (Section 3.3) to parallelly generate  $F_{chunk} = 20$  latent frame video chunks. Each chunk receives  $F_{local} = 8$  local latent frames and 512 global tokens.

**Inference Details:** At inference time, we run reverse diffusion for 50 timesteps using an expanded  $F_{local} = 12$ . We find and later demonstrate through ablations that early token fusion is the most effective and set fusion cutoff ( $t_\alpha = 20$ ).

**Test Set:** We evaluate models on text-to-video generation from a diverse swath of prompts. Our prompt set comprises 150 prompts (Appendix 13) selected by randomly sampling 25 test prompts across six VBench [20] dimensions viz. [subject consistency, background consistency, temporal flickering, temporal style, motion smoothness, overall consistency]. We generate videos at four different lengths, 64, 128, 256, and 512 frames, and sample three videos per prompt for each length to evaluate model performance.

### 4.2. Comparison Methods

Next, we compare VINs to methods across a broad class of video chunk generation paradigms.

**Full Attention (Full):** The pre-trained model generates the entire video simultaneously by attention across all tokens.

**Autoregressive (AutoReg.):** Following prior work [1, 19], we use the replacement with noise method to fine-tune our base model to generate chunks sequentially. We generate 10 latent frames for every step and use 15 context frames.

**StreamingT2V (ST2V):** This state-of-the-art sequential generation technique [17] trains memory modules to facilitate temporal coherency. We compare VINs against their text-to-video implementation <sup>1</sup>.

**FreeNoise:** This parallel inference method [37] uses noise rescheduling and temporal fusion to generate video chunks in parallel. We apply it to our base model with a 20-frame chunk size and 12-frame fusion window.

<sup>1</sup>StreamingModelscape Github Repository

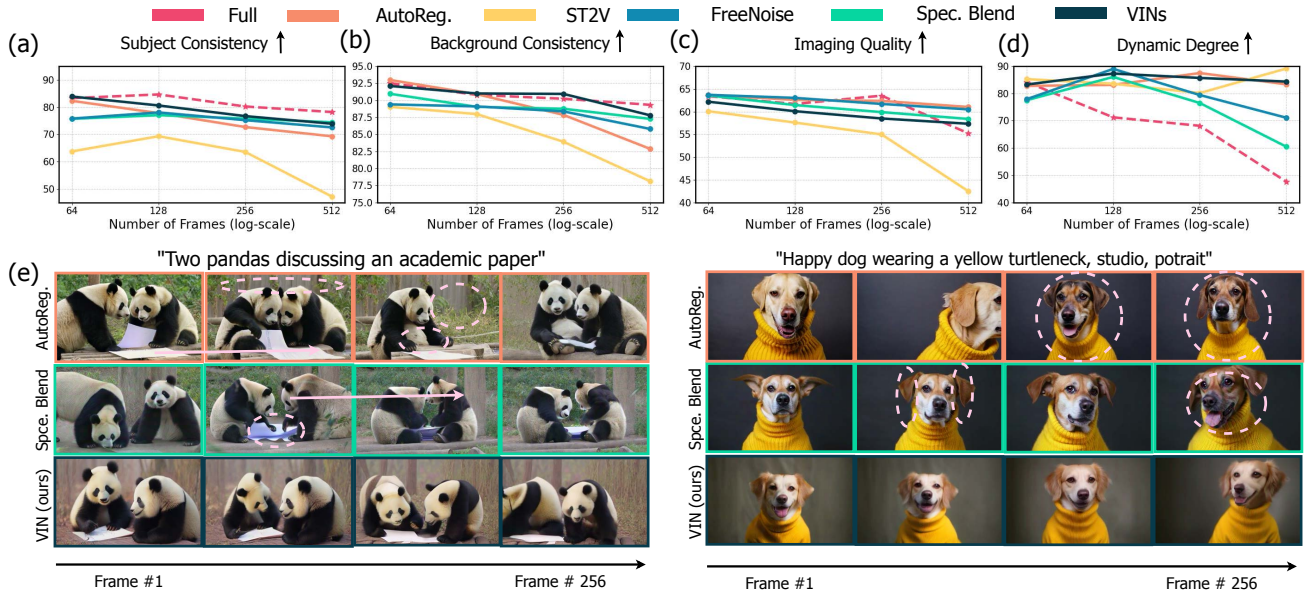


Figure 6. VBench evaluation results. We perform comparisons based on (a) subject consistency, (b) background consistency, (c) imaging quality and (d) dynamic degree. VINs demonstrate superior consistency compared to other chunk-based methods and preserve dynamic degree as opposed to full attention. (d) Visual examples compare VINs against the autoregressive and spectral blending methods on common prompts. VIN samples possess greater semantic consistency, subject identity preservation, and stable backgrounds across frames.

**Spectral Blending (Spec. Blend):** This state-of-the-art parallel inference technique [29] uses band-pass filtering to blend video chunks together. We implemented it on our base model to blend 20-frame chunks together.

### 4.3. VBench Evaluation

Disparate generations of video chunks must preserve temporal consistency, maintaining long-range dependencies across chunks. To this end, we use the VBench Long<sup>2</sup> [20] benchmark to evaluate the long-range consistency and quality of generated videos via four key metrics:

1. **Subject Consistency:** Temporal object consistency using DINOv2 features [33] (‘fast arm’ of VBench Long).
2. **Background Consistency:** Temporal background consistency using CLIP [38] features (‘fast arm’).
3. **Imaging Quality:** Image distortion (over-exposure, blur) using MUSIQ [23].
4. **Dynamic Degree:** Motion magnitude using RAFT optical flow magnitudes [45].

Fig. 6(a), (b), (c) and (d) show the evaluation results across the four dimensions. The major takeaways are as follows:

**VINs improve long-range temporal consistency.** VINs improve subject and background consistency across video chunks, as measured by DINO and CLIP features (Figs. 6(a), (b)), reducing catastrophic forgetting compared to ST2V and an autoregressive baseline. Moreover, VIN meaningfully closes the gap with full generation.

**Full Attention not only stagnates at longer lengths** but paradoxically performs worse despite its quadratic complexity, as evidenced by the deterioration of the Full method

in the dynamic degree plot (Figs. 6 (d)). In contrast, VINs maintains high dynamic degree and temporal consistency throughout long videos while remaining efficient.

**VINs trade off temporal consistency for subject-aware softening.** We observed that while VINs maintain subject fidelity, they exhibit a marginal difference in image quality, as reflected in the scores of Fig. 6(c). However, the quality remains competitive with other techniques, also validated by the user study in Section 4.6.

**Visual examples.** Fig. 6(e) illustrates our observations via four diverse prompts. We notice that VIN-generated videos have greater subject and background stability and preserve the relative positions of the objects in the scene. See Appendix 7 for more evaluations and Appendix 8 for qualitative visualizations.

### 4.4. Optical Flow Analysis

While VINs demonstrate consistency as measured by deep neural network features, such a consistency should also reliably transfer to pixel-level generation. To this end, this section analyzes the optical flow across generated frames with the RAFT model [45].

**Metrics.** We adopt the MAWE metric [17], which, for a video  $V$ , is defined as  $W(V)/(c \times OFS(V))$ , where  $W(V)$  measures the average squared L2 pixel distance between a frame and its corresponding warped frame, excluding occluded regions,  $OFS(V)$  computes the mean magnitude of optical flow vectors between consecutive frames, and  $c = 9.5$  is the calibration constant. A low MAWE score suggests that the generated video exhibits temporal coherency, with high optical magnitudes. In addition, we

<sup>2</sup>VBench Long Github Repository

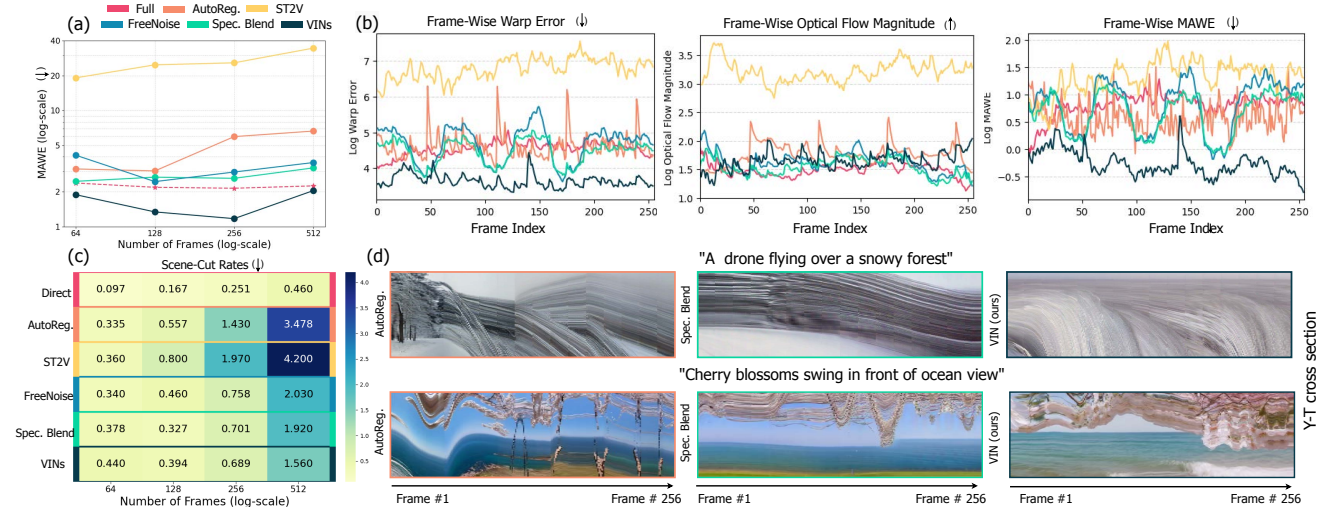


Figure 7. Optical Flow Analysis: (a) VINs demonstrate more consistent and natural-looking movement. They outperform the MAWE scores of the state of the art by a significant margin. (b) Per-frame optical flow analysis shows that VIN-generated videos simultaneously have low warp error and considerable optical flow, implying smooth and dynamic videos. (c) In addition, VINs also reduce abrupt scene changes. (d) Visualizing  $y-t$  cross-section of generated videos reveals motion smoothness endowed by VIN.

also use PySceneDetect [4] to detect abrupt scene changes and report **Scene-Cut Rates** per video. Fig. 7 reports the results of the analysis. We highlight some key observations.

**VINs outperform previous techniques in terms of motion consistency.** Fig. 7(a) shows that VINs maintain a considerably lower MAWE across different video lengths, with scores consistently remaining below 2.0 even at 512 frames, in contrast to baseline methods. Note that other methods that use the same base model do not exhibit this improvement. Fig. 7(b) shows frame-wise MAWE, warping error, and optical flow. VINs exhibit stable optical flow (1.5-2.0) and consistently lower warping errors (4.0-5.0) compared to others, which have more erratic and bursty motion.

**VINs maintain scene continuity across video chunks at longer lengths.** The heatmap in Fig. 7(c) demonstrates that, compared to other chunking methods, VINs achieve the lowest scene-cut detection rates for longer video lengths of 256 and 512 frames, minimizing the performance gap between chunked and direct video generation. Fig. 7(d) visualizes the  $y-t$  cross-section of 256 frame videos generated by VINs and the Autoregressive method. VINs demonstrate smoother transitions with fewer aberrations.

**Consistency across chunk transitions.** We specifically analyzed consistency across chunk boundaries in Fig. 8 by measuring the warp error and MAWE around chunk transitions. In addition, we estimated the gold standard baseline by measuring transition errors from ground truth decoded latents obtained from the 3D VAE (Oracle). Our method achieves comparable warp error to full attention and significantly reduces the MAWE gap with the Oracle. Fig. 9 visualizes the smooth chunk transitions on generated videos.

**Comparison to Full Attention.** Video generators face a natural tradeoff between temporal consistency and motion

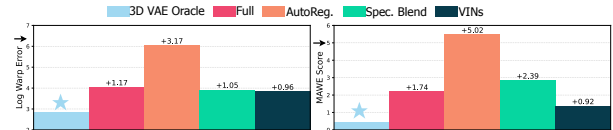


Figure 8. Optical flow analysis of chunk transitions in 256 frame videos. Measured over  $\Delta = 16$  frames before chunk boundary. Numbers above the bars show gap from the 3D VAE Oracle.

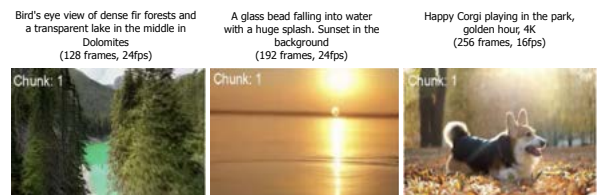


Figure 9. Chunk Transition Visualization. Generated videos show a chunk counter on the top left. A red dot appears on the top right before chunk boundaries.

dynamism. Our analysis in Fig. 10 (a) demonstrates that VINs achieve a superior balance in this tradeoff, particularly as frame counts increase. Naively extending DiT context with full attention diminishes motion and causes repetitions due to diluted temporal connections (see Appendix 8). Beyond motion quality, our approach addresses critical scalability limitations of full attention. As illustrated in Fig. 10 (b), VINs deliver 25-40% higher efficiency (also Fig. 1) and 40-75% faster denoising speeds while requiring only marginally more memory, making them significantly more practical for longer video generation.

#### 4.5. VIN Ablations and Interpretability

**Ablations.** Table 1 presents the results of ablation experiments on key VIN architectural components. **The full model achieved the best overall performance**, while

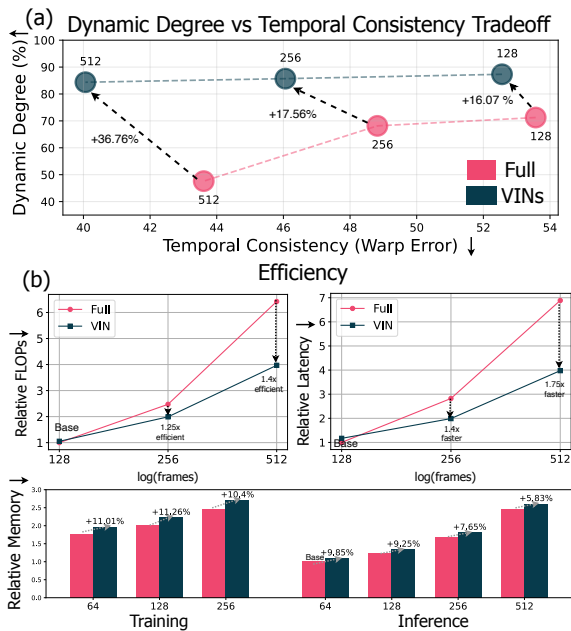


Figure 10. Comparison to full attention: (a) VIN maintains a superior consistency-dynamic degree tradeoff across different frames. (b) Efficiency analysis of the full vs. VIN model. Latency and memory are measured on NVIDIA A100 80GB GPU using the same memory-efficient transformer implementation.

**removing global tokens significantly reduced temporal consistency.** Past works [24] have posited that diffusion models form object-structure features early in the sampling process; thus, our **full model benefited from early fusion** compared to other fusion schedules. **Expanding the local context at inference time also improves motion flow.** Interestingly, increasing the number of keyframes sampled does not improve consistency, suggesting redundancy of dense temporal sampling for VINs.

**VIN Interpretability.** We interpret learned VIN representations by visualizing the attention distribution across input video keys (Fig. 11). The distributions revealed semantically meaningful attention patterns, with heads focusing on human forms, architecture, and objects. See Appendix 10 for attention across entire videos.

Model Configuration	MAWE ↓	Scene Cuts ↓
Full Model	<b>1.09</b>	<b>0.21</b>
w/o Global Tokens	1.69	0.33
w/o fusion	1.13	1.00
Mid fusion ( $t_\alpha, t_\beta = 35, 15$ )	1.11	0.33
Late fusion ( $t_\alpha = 20$ )	1.22	0.74
Local Frames - 8 \ 10	1.51 \ 1.17	0.24 \ 0.22
Keyframe $T_s - 0.5s \ 0.2s$	1.14 \ 1.21	0.34 \ 0.29

Table 1. Effect of model ablations on motion consistency.

#### 4.6. User Study

We set up a user study (design outlined in Appendix 12) where a cohort of humans was asked to compare videos

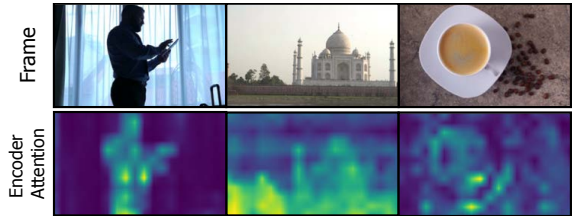


Figure 11. VIN Interpretability. VIN attention heads focus on semantically meaningful objects in the scene.

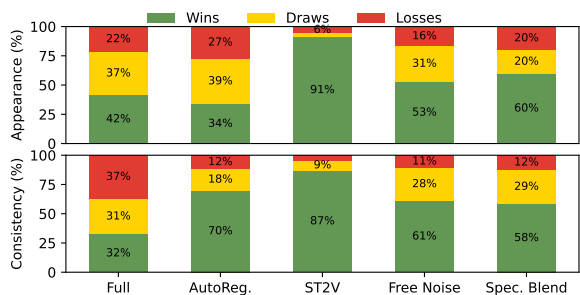


Figure 12. User study results.

generated by VINs against other methods on (1) overall appearance and (2) temporal consistency. Fig. 12 reports the percentage results with which VIN is deemed better, comparable, or worse. In contrast to the imaging quality results of Section 4.3, humans rated VIN-generated videos to be comparable on average or even better (loss rate < 30%). Moreover, the judged temporal consistency largely correlates with the VBench results, where VIN preference matches full generation, substantially improves upon parallel methods, and outperforms sequential generation.

#### 4.7. Discussion

**Dynamic universal representations enable long-range video consistency.** Unlike context-limited autoregressive methods [1, 19] or static priors [17], VINs use global tokens recomputed each step, degrading gracefully with video length. **Deep hierarchical priors improve motion smoothness.** Compared to surface-level priors (FreeNoise [37], Spectral Blending [29]) and DiT, VINs achieve lower MAWE scores, suggesting deep semantic representations enable fluid long-video motion. **Limitations:** VINs only learn through generation. Future work could explore concurrent learning on downstream tasks for richer representations and depth/3D input beyond raw patches.

### 5. Conclusion

We proposed a paradigm to parallelize inference on videos by using global tokens from long videos to denoise shorter video chunks. Our experiments show that this hierarchy improves subject and background consistency across chunks, endows fluid motion, and surpasses other state-of-the-art chunking techniques. Compared to full attention, VIN improves the consistency-motion dynamism tradeoff besides being scalable. The generated videos are also judged favorably by human raters.



## References

- [1] Andreas Blattmann, Tim Dockhorn, Sumith Kulal, Daniel Mendelevitch, Maciej Kilian, Dominik Lorenz, Yam Levi, Zion English, Vikram Voleti, Adam Letts, Varun Jampani, and Robin Rombach. Stable Video Diffusion: Scaling Latent Video Diffusion Models to Large Datasets. *CoRR*, abs/2311.15127, 2023. 2, 5, 8
- [2] Andreas Blattmann, Robin Rombach, Huan Ling, Tim Dockhorn, Seung Wook Kim, Sanja Fidler, and Karsten Kreis. Align your Latents: High-Resolution Video Synthesis with Latent Diffusion Models. *CoRR*, abs/2304.08818, 2023. 2
- [3] Tim Brooks, Bill Peebles, Connor Holmes, Will DePue, Yufei Guo, Li Jing, David Schnurr, Joe Taylor, Troy Luhman, Eric Luhman, Clarence Ng, Ricky Wang, and Aditya Ramesh. Video Generation Models as World Simulators. *OpenAI Research Blog*, 2024. 1, 2
- [4] Brandon Castellano. PySceneDetect: Video Cut Detection and Analysis Tool. <https://github.com/Breakthrough/PySceneDetect>, 2024. 7
- [5] Junsong Chen, Jincheng Yu, Chongjian Ge, Lewei Yao, Enze Xie, Yue Wu, Zhongdao Wang, James Kwok, Ping Luo, Huchuan Lu, and Zhenguo Li. PixArt- $\alpha$ : Fast Training of Diffusion Transformer for Photorealistic Text-to-Image Synthesis. *CoRR*, abs/2310.00426, 2023. 1
- [6] Xinyuan Chen, Yaohui Wang, Lingjun Zhang, Shaobin Zhuang, Xin Ma, Jiashuo Yu, Yali Wang, Dahua Lin, Yu Qiao, and Ziwei Liu. SEINE: Short-to-Long Video Diffusion Model for Generative Transition and Prediction. *CoRR*, abs/2310.20700, 2023. 2
- [7] Zuozhuo Dai, Zhenghao Zhang, Yao Yao, Bingxue Qiu, Siyu Zhu, Long Qin, and Weizhi Wang. AnimateAnything: Fine-Grained Open Domain Image Animation with Motion Guidance. *CoRR*, abs/2311.12886, 2023.
- [8] Patrick Esser, Johnathan Chiu, Parmida Atighehchian, Jonathan Granskog, and Anastasis Germanidis. Structure and Content-Guided Video Synthesis with Diffusion Models. *CoRR*, abs/2302.03011, 2023. 2
- [9] Adam Polyak et al. Movie Gen: A Cast of Media Foundation Models. *CoRR*, abs/2410.13720, 2024. 1, 2
- [10] Weijie Kong et al. HunyuanVideo: A Systematic Framework for Large Video Generative Models. *CoRR*, abs/2412.03603, 2024. 1, 2
- [11] Zhiyu Tan et al. VidGen-1M: A Large-Scale Dataset for Text-to-video Generation. *CoRR*, abs/2408.02629, 2024.
- [12] Jonathan St. B. T. Evans. Dual-processing Accounts of Reasoning, Judgment, and Social Cognition. *Annual Review of Psychology*, 59:255–278, 2008. 2
- [13] Yuwei Guo, Ceyuan Yang, Anyi Rao, Maneesh Agrawala, Dahua Lin, and Bo Dai. SparseCtrl: Adding Sparse Controls to Text-to-Video Diffusion Models. *CoRR*, abs/2311.16933, 2023. 2
- [14] Yuwei Guo, Ceyuan Yang, Anyi Rao, Zhengyang Liang, Yaohui Wang, Yu Qiao, Maneesh Agrawala, Dahua Lin, and Bo Dai. AnimateDiff: Animate Your Personalized Text-to-Image Diffusion Models without Specific Tuning. *CoRR*, abs/2307.04725, 2024. 2
- [15] Agrim Gupta, Lijun Yu, Kihyuk Sohn, Xiuye Gu, Meera Hahn, Li Fei-Fei, Irfan Essa, Lu Jiang, and José Lezama. Photorealistic Video Generation with Diffusion Models. *CoRR*, abs/2312.06662, 2023. 2
- [16] Yingqing He, Tianyu Yang, Yong Zhang, Ying Shan, and Qifeng Chen. Latent Video Diffusion Models for High-Fidelity Long Video Generation. *CoRR*, abs/2211.13221, 2023. 2
- [17] Roberto Henschel, Levon Khachatryan, Daniil Hayrapetyan, Hayk Poghosyan, Vahram Tadevosyan, Zhangyang Wang, Shant Navasardyan, and Humphrey Shi. StreamingT2V: Consistent, Dynamic, and Extendable Long Video Generation from Text. *CoRR*, abs/2403.14773, 2024. 1, 2, 5, 6, 8
- [18] Jonathan Ho, Ajay Jain, and Pieter Abbeel. Denoising Diffusion Probabilistic Models. *CoRR*, abs/2006.11239, 2020. 2
- [19] Jonathan Ho, Tim Salimans, Alexey Gritsenko, William Chan, Mohammad Norouzi, and David J. Fleet. Video Diffusion Models. *CoRR*, abs/2204.03458, 2022. 2, 5, 8
- [20] Ziqi Huang, Yanan He, Jiashuo Yu, Fan Zhang, Chenyang Si, Yuming Jiang, Yuanhan Zhang, Tianxing Wu, Qingyang Jin, Nattapol Chanpaisit, Yaohui Wang, Xinyuan Chen, Limin Wang, Dahua Lin, Yu Qiao, and Ziwei Liu. VBench: Comprehensive Benchmark Suite for Video Generative Models. *CoRR*, abs/2311.17982, 2023. 2, 5, 6, 1
- [21] Allan Jabri, David Fleet, and Ting Chen. Scalable Adaptive Computation for Iterative Generation. *CoRR*, abs/2212.11972, 2023. 3
- [22] Daniel Kahneman. Thinking, Fast and Slow. *Farrar, Straus and Giroux*, 2011. 2
- [23] Junjie Ke, Qifei Wang, Yilin Wang, Peyman Milanfar, and Feng Yang. MUSIQ: Multi-scale Image Quality Transformer. *CoRR*, abs/2108.05997, 2021. 6
- [24] Yulhwa Kim, Dongwon Jo, Hyesung Jeon, Taesu Kim, Dae-hyun Ahn, Hyungjun Kim, and Jae-Joon Kim. Leveraging Early-Stage Robustness in Diffusion Models for Efficient and High-Quality Image Synthesis. In *Advances in Neural Information Processing Systems*, pages 1229–1244. Curran Associates, Inc., 2023. 8
- [25] Diederik P. Kingma and Max Welling. Auto-Encoding Variational Bayes. *CoRR*, abs/1312.6114, 2022. 5
- [26] Shenggui Li, Fuzhao Xue, Chaitanya Baranwal, Yongbin Li, and Yang You. Sequence Parallelism: Long Sequence Training from System Perspective. *CoRR*, abs/2105.13120, 2022. 2
- [27] Zhen Li, Zuo-Liang Zhu, Ling-Hao Han, Qibin Hou, Chun-Le Guo, and Ming-Ming Cheng. AMT: All-Pairs Multi-Field Transforms for Efficient Frame Interpolation. *CoRR*, abs/2304.09790, 2023. 1
- [28] Fuchen Long, Zhaofan Qiu, Ting Yao, and Tao Mei. VideoStudio: Generating Consistent-Content and Multi-Scene Videos. *CoRR*, abs/2401.01256, 2024. 3
- [29] Yu Lu, Yuanzhi Liang, Linchao Zhu, and Yi Yang. Free-Long: Training-Free Long Video Generation with Spectral-Blend Temporal Attention. *CoRR*, abs/2407.19918, 2024. 2, 3, 6, 8

- [30] Xin Ma, Yaohui Wang, Gengyun Jia, Xinyuan Chen, Ziwei Liu, Yuan-Fang Li, Cunjian Chen, and Yu Qiao. Latte: Latent Diffusion Transformer for Video Generation. *CoRR*, abs/2401.03048, 2024. [2](#)
- [31] Shentong Mo, Enze Xie, Ruihang Chu, Lewei Yao, Lanqing Hong, Matthias Nießner, and Zhenguo Li. DiT-3D: Exploring Plain Diffusion Transformers for 3D Shape Generation. *CoRR*, abs/2307.01831, 2023. [1](#)
- [32] Gyeongrok Oh, Jaehwan Jeong, Sieun Kim, Wonmin Byeon, Jinkyu Kim, Sungwoong Kim, and Sangpil Kim. MEVG: Multi-event Video Generation with Text-to-Video Models. *CoRR*, abs/2312.04086, 2024. [2](#)
- [33] Maxime Oquab, Timothée Darcet, Théo Moutakanni, Huy Vo, Marc Szafraniec, Vasil Khalidov, Pierre Fernandez, Daniel Haziza, Francisco Massa, Alaaeldin El-Nouby, Mahmoud Assran, Nicolas Ballas, Wojciech Galuba, Russell Howes, Po-Yao Huang, Shang-Wen Li, Ishan Misra, Michael Rabbat, Vasu Sharma, Gabriel Synnaeve, Hu Xu, Hervé Jegou, Julien Mairal, Patrick Labatut, Armand Joulin, and Piotr Bojanowski. DINOv2: Learning Robust Visual Features without Supervision. *CoRR*, abs/2304.07193, 2024. [6](#)
- [34] William Peebles and Saining Xie. Scalable Diffusion Models with Transformers. *CoRR*, abs/2212.09748, 2023. [1](#), [2](#)
- [35] Pablo Pernias, Dominic Rampas, Mats L. Richter, Christopher J. Pal, and Marc Aubreville. Wuerstchen: An Efficient Architecture for Large-Scale Text-to-Image Diffusion Models. *CoRR*, abs/2306.00637, 2023. [3](#)
- [36] Konpat Preechakul, Nattanat Chatthee, Suttisak Wizadwongsa, and Supasorn Suwajanakorn. Diffusion Autoencoders: Toward a Meaningful and Decodable Representation. *CoRR*, abs/2111.15640, 2022. [3](#)
- [37] Haonan Qiu, Menghan Xia, Yong Zhang, Yingqing He, Xintao Wang, Ying Shan, and Ziwei Liu. FreeNoise: Tuning-Free Longer Video Diffusion via Noise Rescheduling. *CoRR*, abs/2310.15169, 2024. [2](#), [3](#), [5](#), [8](#)
- [38] Alec Radford, Jong Wook Kim, Chris Hallacy, Aditya Ramesh, Gabriel Goh, Sandhini Agarwal, Girish Sastry, Amanda Askell, Pamela Mishkin, Jack Clark, Gretchen Krueger, and Ilya Sutskever. Learning Transferable Visual Models from Natural Language Supervision. *CoRR*, abs/2103.00020, 2021. [6](#)
- [39] Samyam Rajbhandari, Jeff Rasley, Olatunji Ruwase, and Yuxiong He. ZeRO: Memory Optimizations Toward Training Trillion Parameter Models. *CoRR*, abs/1910.02054, 2020. [2](#)
- [40] Robin Rombach, Andreas Blattmann, Dominik Lorenz, Patrick Esser, and Björn Ommer. High-Resolution Image Synthesis with Latent Diffusion Models. *CoRR*, abs/2112.10752, 2022. [2](#)
- [41] Mohammad Shoeybi, Mostofa Patwary, Raul Puri, Patrick LeGresley, Jared Casper, and Bryan Catanzaro. Megatron-LM: Training Multi-Billion Parameter Language Models Using Model Parallelism. *CoRR*, abs/1909.08053, 2020. [2](#)
- [42] Steven A. Sloman. The Empirical Case for Two Systems of Reasoning. *Psychological Bulletin*, 119(1):3–22, 1996. [2](#)
- [43] Jascha Sohl-Dickstein, Eric A. Weiss, Niru Maheswaranathan, and Surya Ganguli. Deep Unsupervised Learning using Nonequilibrium Thermodynamics. *CoRR*, abs/1503.03585, 2015. [2](#)
- [44] Genmo Team. Mochi. <https://www.genmo.ai/blog>, 2024. [1](#), [2](#)
- [45] Zachary Teed and Jia Deng. RAFT: Recurrent All-Pairs Field Transforms for Optical Flow. *CoRR*, abs/2003.12039, 2020. [6](#), [1](#)
- [46] Fu-Yun Wang, Wenshuo Chen, Guanglu Song, Han-Jia Ye, Yu Liu, and Hongsheng Li. Gen-L-Video: Multi-Text to Long Video Generation via Temporal Co-Denoising. *CoRR*, abs/2305.18264, 2023. [3](#)
- [47] Jiuniu Wang, Hangjie Yuan, Dayou Chen, Yingya Zhang, Xiang Wang, and Shiwei Zhang. ModelScope Text-to-Video Technical Report. *CoRR*, abs/2308.06571, 2023. [2](#), [1](#)
- [48] Xiang Wang, Hangjie Yuan, Shiwei Zhang, Dayou Chen, Jiuniu Wang, Yingya Zhang, Yujun Shen, Deli Zhao, and Jingren Zhou. VideoComposer: Compositional Video Synthesis with Motion Controllability. *CoRR*, abs/2306.02018, 2023. [2](#)
- [49] Yi Wang, Yanan He, Yizhuo Li, Kunchang Li, Jiashuo Yu, Xin Ma, Xinhao Li, Guo Chen, Xinyuan Chen, Yaohui Wang, Conghui He, Ping Luo, Ziwei Liu, Yali Wang, Limin Wang, and Yu Qiao. InternVid: A Large-scale Video-Text Dataset for Multimodal Understanding and Generation. *CoRR*, abs/2307.06942, 2024. [1](#)
- [50] Jinbo Xing, Menghan Xia, Yong Zhang, Haoxin Chen, Wangbo Yu, Hanyuan Liu, Xintao Wang, Tien-Tsin Wong, and Ying Shan. DynamicCrafter: Animating Open-domain Images with Video Diffusion Priors. *CoRR*, abs/2310.12190, 2023. [2](#)
- [51] Yan Zeng, Guoqiang Wei, Jiani Zheng, Jiaxin Zou, Yang Wei, Yuchen Zhang, and Hang Li. Make Pixels Dance: High-Dynamic Video Generation. *CoRR*, abs/2311.10982, 2023. [2](#)
- [52] Shiwei Zhang, Jiayu Wang, Yingya Zhang, Kang Zhao, Hangjie Yuan, Zhiwu Qin, Xiang Wang, Deli Zhao, and Jingren Zhou. I2VGen-XL: High-Quality Image-to-Video Synthesis via Cascaded Diffusion Models. *CoRR*, abs/2311.04145, 2023. [2](#)
- [53] Yanli Zhao, Andrew Gu, Rohan Varma, Liang Luo, Chien-Chin Huang, Min Xu, Less Wright, Hamid Shojanazeri, Myle Ott, Sam Shleifer, Alban Desmaison, Can Balioglu, Pritam Damania, Bernard Nguyen, Geeta Chauhan, Yuchen Hao, Ajit Mathews, and Shen Li. PyTorch FSDP: Experiences on Scaling Fully Sharded Data Parallel. *CoRR*, abs/2304.11277, 2023. [2](#)
- [54] Zangwei Zheng, Xiangyu Peng, Tianji Yang, Chenhui Shen, Shenggui Li, Hongxin Liu, Yukun Zhou, Tianyi Li, and Yang You. Open-Sora: Democratizing Efficient Video Production for All. <https://github.com/hpcaitech/Open-Sora>, 2024. [1](#), [5](#), [2](#)

# Generating, Fast and Slow: Scalable Parallel Video Generation with Video Interface Networks

## Supplementary Material

The index.html attached to the supplementary folder displays all the videos reported in this work.

### 6. Comparison to Open Weight Models

We compared our approach to three open weight DIT models viz. OpenSora v1.2 [54], Mochi-1 [44] and Hunyuan-Video [10] using full attention on the long video. We analyzed videos generated at the 256 frame setting on different VBench metrics in Table 2. While OpenSora has been natively trained to generate longer videos, both Mochi-1 and HunyuanVideo were evaluated at the extended frame setting where inference was performed beyond the recommended number of frames. As a strong baseline, we also report the results from using our base model in the extended setting. Our primary finding was that at longer frame settings, all the DiT models exhibit stagnated motion in the video where temporal dynamics often become near static. As a result, while this leads to high consistency scores, the dynamic degree suffers significantly. This corroborates our findings in the main section where our base model also exhibits this detrimental tradeoff. Moreover, VIN not only maintains consistency at par with the open models but also outperforms them on the dynamic degree metric by a significant margin. We also noticed that outputs from both Mochi-1 and Hunyuan video qualitatively deteriorate at longer frame settings, with the latter also showing temporal flickering artifacts. Fig. 14 and 15 show the qualitative comparisons between models.

### 7. Additional VBench Evaluation Metrics

We also evaluated generated videos from different chunk based methods on two other VBench [20] metrics, {Text-Video Alignment, Motion Smoothness, Dynamic Degree}, as shown in Fig. 13. We observed the following:

1. **Text-Video Alignment:** Alignment scores, as measured by ViCLIP [49], were primarily bifurcated by the base model. StreamingT2V [17] that uses a ModelScope [47] base has a considerably lower score than the other methods, which use a common base model. Overall, text-video alignment scores diminish with video length, with the autoregression scores deteriorating more than the other parallel inference and full-generation methods.
2. **Motion Smoothness:** VBench measures motion smoothness via motion priors obtained from a frame interpolation model [27]. We observe that the motion smoothness of our model is uniformly high across all evaluations. In principle, this metric captures the essence of pixel-level motion fluidity similar to our experiment

in Section 4.4; however, it fundamentally differs in the motion-prior we utilize. The AMT model, on which the VBench metric is based, uses bidirectional correlation volumes and regresses on frame interpolation and, therefore, reasons about coarser flows in the video. On the other hand, we use the RAFT [45] model that is trained to measure the optical flow of each pixel and gives a more faithful measure of finer flows across frames. The difference in motion smoothness measured by the former is, therefore, less apparent compared to RAFT, where the difference is much more pronounced.

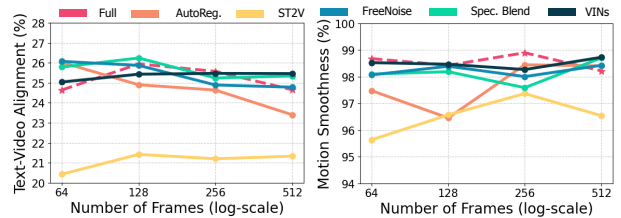


Figure 13. VBench evaluation results on Text-Video alignment, motion smoothness, and dynamic degree of the video.

### 8. Qualitative Visualization

Figs. 16-20 demonstrate videos generated by VINs and other methods considered in this paper over different prompts. Figs. 16, 17, 18 show the generations on prompts that primarily consist of diverse objects or background details where semantic coherence is crucial. We observe that VINs maintain the subject, object, and background consistency while also generating more photorealistic videos. We also notice the subject-aware softening mentioned in Section 4.3. This was specifically observed where the prompt’s background description was missing. For example, “A Raccoon Dressed in a Suit Playing the Trumpet,” and “Grizzly Bear Trying to Learn Calculus.” Figs. 19 and 20 show the generated videos on landscape prompts along with their  $y-t$  cross-sections. As evidenced by the latter visualizations, the perturbations across chunk boundaries for VINs are minimal and the transitions are smoother. As highlighted in Fig. 10 (a), one can also qualitatively observe the disparity of the consistency-dynamic degree tradeoff between full attention and VINs. Full attention methods tend to generate outputs with undesirable artifacts more often than not. These frequently manifest as reduced motion, diminished object complexity, and loopy distortions, exemplified by the “Grizzly bear,” “Dog wearing a cape,” “Rabbit in a fantasy landscape,” and “Shark in the ocean” prompts.

Model	Extended Setting	Subj. Consist.	BG Consist.	Imag. Qual.	Temp. Flicker.	Motion Smooth.	Dyna. Degree	Text-Video Align.
OpenSora v1.2 [54]	No	96.75%	97.61%	56.85%	99.53%	98.50%	63.34%	<b>26.85%</b>
Mochi-1 [44]	Yes (163 → 256)	96.99%	97.28%	56.94%	99.40%	97.02%	60.64%	25.15%
HunyuanVideo [10]	Yes (128 → 256)	<b>97.37 %</b>	<b>97.76 %</b>	54.39 %	98.32%	97.96%	70.83%	26.44%
Base DiT (Ours)	Yes (128 → 256)	96.91 %	97.20 %	<b>63.52 %</b>	<b>99.64%</b>	<b>98.57%</b>	68.15%	25.57%
VINs (Ours)	No	96.4%	97.13%	58.5 %	99.12%	<b>98.55 %</b>	<b>87.32 %</b>	25.43%

Table 2. Comparison of VINs against Open Weight DiT Models. We considered three popular open weight models and evaluated them on key VBench metrics at the 256-frame settings. Inference was performed via the Full attention mode. While most models exhibit good consistency at long frames, they tend to often stagnate and become static, leading to poor dynamic degree scores.

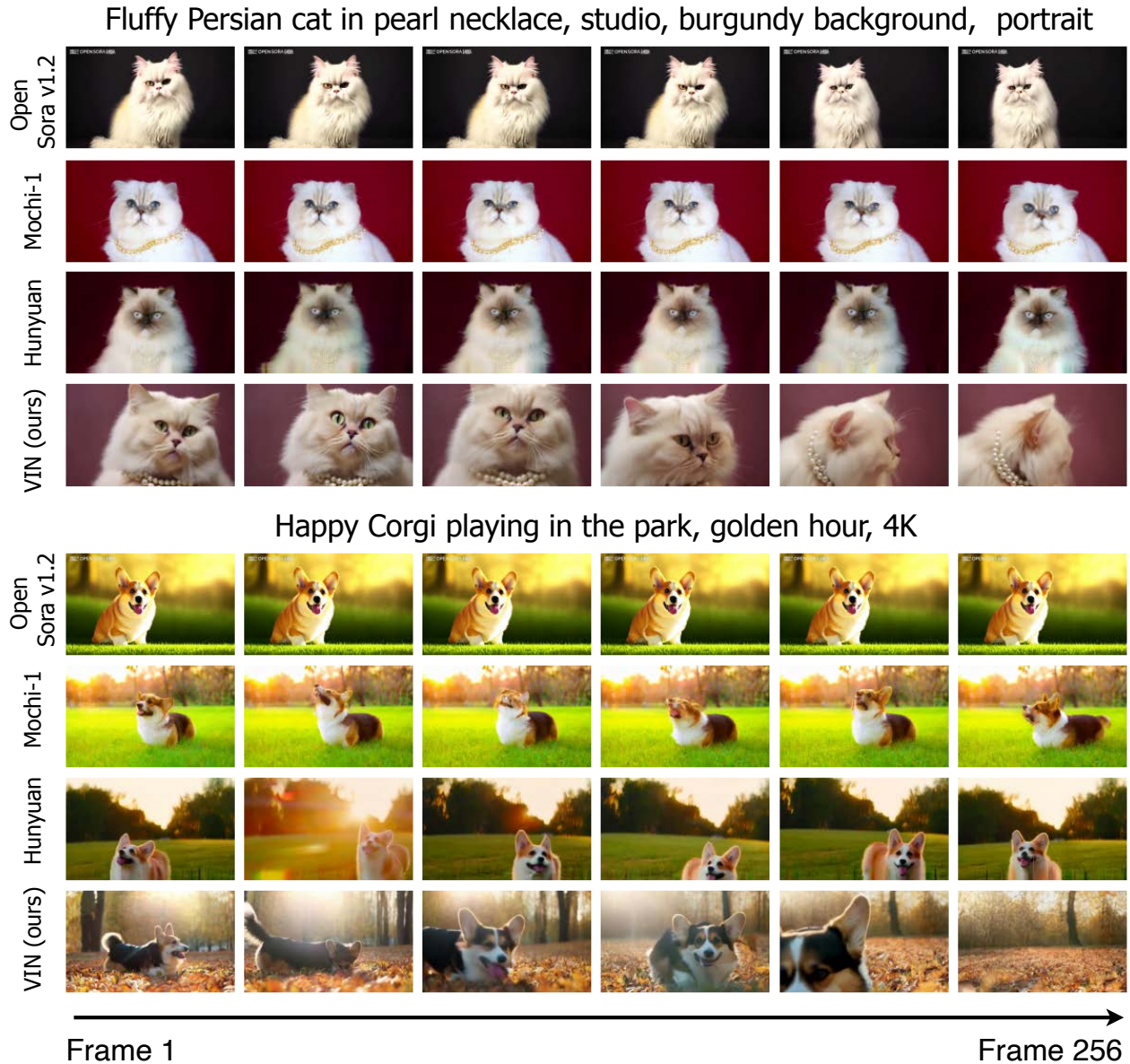


Figure 14. Qualitative comparison of VINs against open weight models at 256 frames.

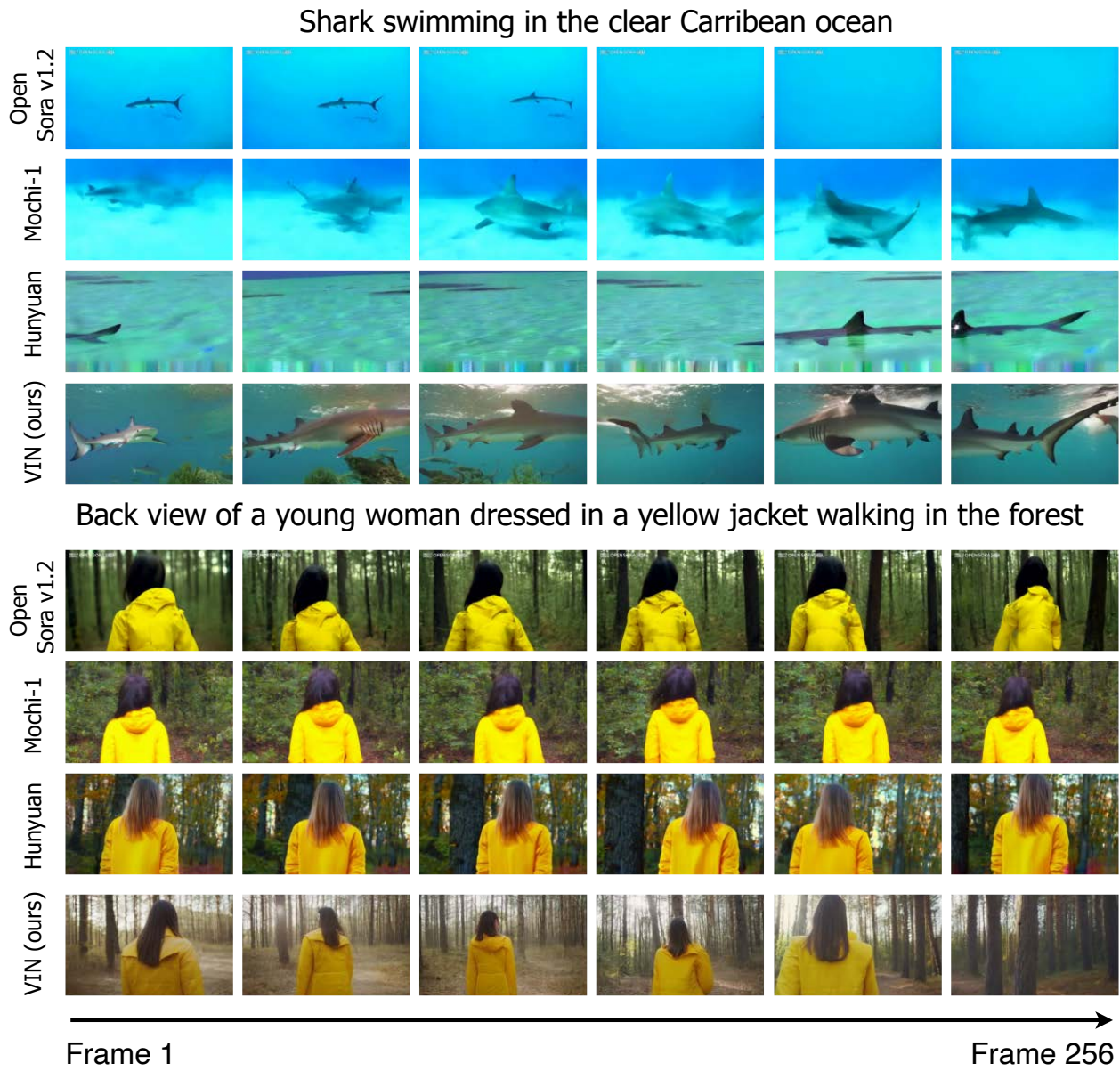


Figure 15. Qualitative comparison of VINs against open weight models at 256 frames.

Confused grizzly bear trying to learn Calculus



Back view of a young woman dressed in a yellow jacket walking in the forest



Figure 16. Qualitative visualizations across different methods.

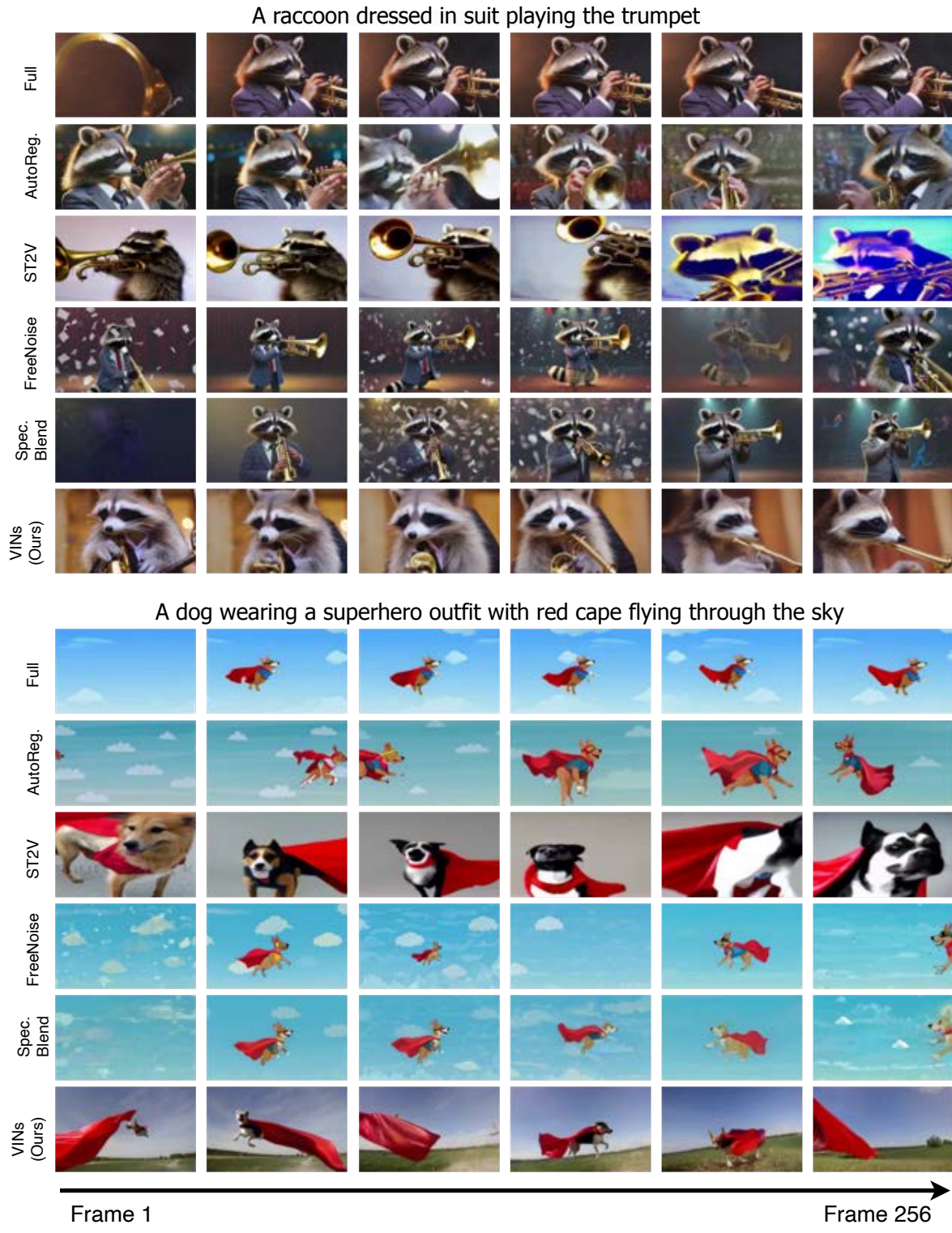


Figure 17. Qualitative visualizations across different methods.

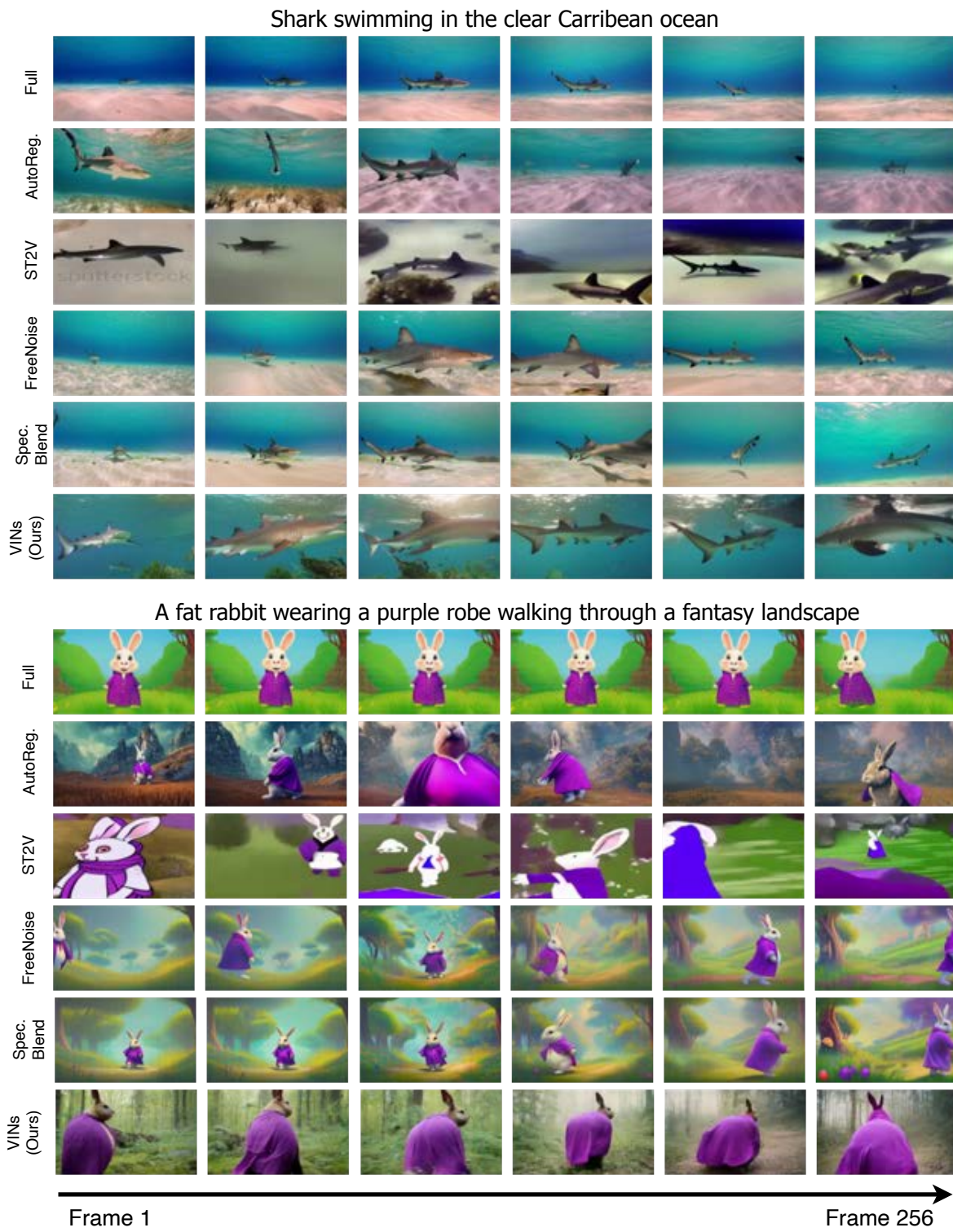


Figure 18. Qualitative visualizations across different methods.



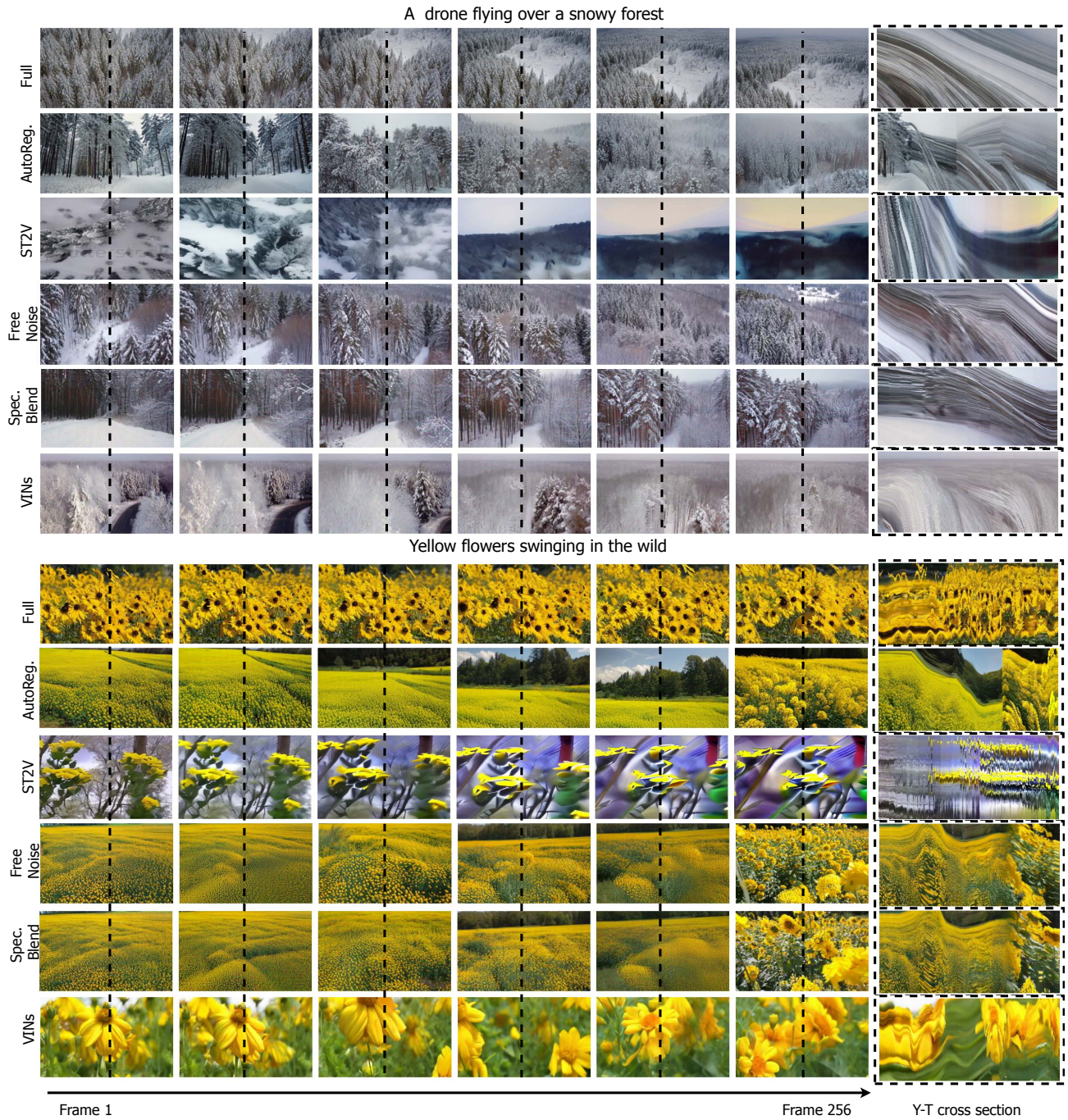


Figure 19. Qualitative visualizations across different methods.

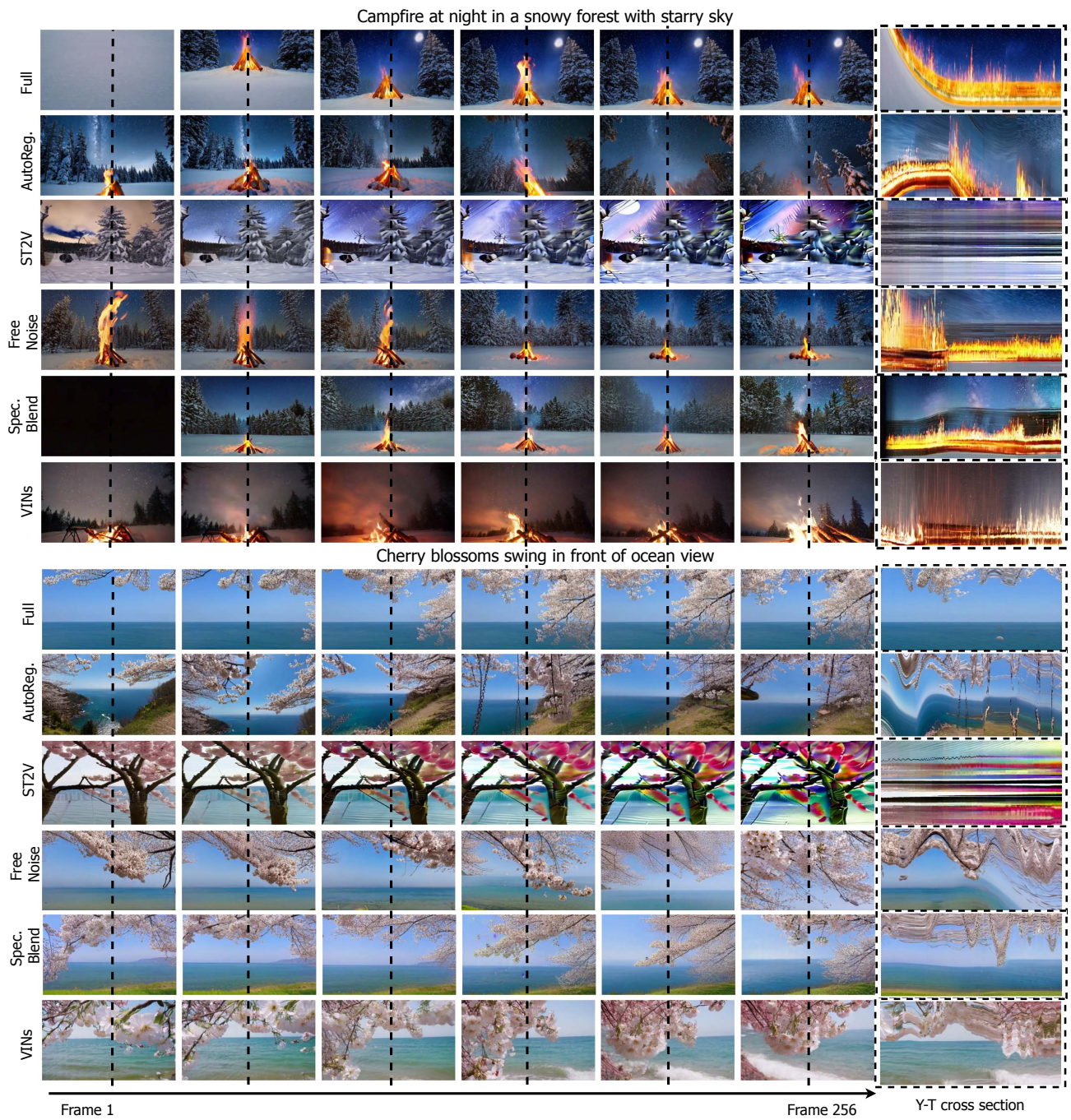


Figure 20. Qualitative visualizations across different methods.

## 9. Additional Ablation Results

**Ablation Experiments Setup.** We used a smaller subset of prompts from the VBench suite for the ablation experiments. We extracted 25 prompts from the overall consistency prompts and, for each variant of the ablated model, generated two samples per prompt.

**Global Token Ablation.** Fig. 21 shows the effect of the global tokens. We ran the sampling chain under two settings: (1) global tokens and (2) without global tokens, initialized from the same noise. Identities of subjects in videos generated without global tokens tend to drift in subsequent frames.

## 10. Qualitative Interpretability

Figs. 22 and 23 show the VIN encoder attention maps on inputs. Fig. 22 displays the temporal dynamics of the attention patterns across videos. At the beginning of the video, attention is assigned to all objects within the scene. However, as the video progresses, we observe motion-aware encoding such that only the objects in motion are weighed significantly by the attention heads. For example, in the first example of Fig. 22, the attention heads focus on the man and the suitcase nearby and stay focused as the camera pans upward. As the camera stops and only the arms of the man move, attention from the suitcase is removed and transferred to the moving limbs. Similarly, in the third example, the attention pivots from the broader scene to the fingers and scissors in active motion while cutting the vegetables. Fig. 23 shows the object-centric attention over individual frames across different videos.

## 11. Training and Inference Algorithms for VINs

Algorithms 1 and 2 detail the training and inference algorithm, respectively, for the VIN-DiT coupling.

---

### Algorithm 1 Training with VIN $\leftrightarrow$ DiT ensemble at $t$

---

**Require:** Noisy tokenized input  $X_t$  from  $\epsilon_t \sim \mathcal{N}(\mathbf{0}, \mathbf{I})$

**Require:**  $N_s$  chunk size,  $N_{local}$  local size

```

 $Z_t \leftarrow f_\alpha(X_t, t)$  ▷ Encode  $X_t$  via VINs
for  $i = 0, \dots, \lfloor N/N_s \rfloor$  do ▷ Run in Parallel
   $X_t^i \leftarrow X_t[:, iN_s : (i+1)N_s]$ 
   $X_t^{local} \leftarrow X_t[:, iN_s - N_{local} : iN_s].detach()$ 
   $\hat{\epsilon}_t^i \leftarrow \epsilon_\theta(\text{concat}[X_t^{local}, X_t^i, Z_t], t)$  ▷ Denoise
   $\hat{\epsilon}_t^i \leftarrow \hat{\epsilon}_t^i[:, N_{local} : N_{local} + N_s]$  ▷ Drop tokens
end for

```

```

 $\hat{\epsilon}_t = \text{concat}[\hat{\epsilon}_t^0, \dots, \hat{\epsilon}_t^{\lfloor N/N_s \rfloor}]$ 

```

```

Gradient step on  $\nabla_{\alpha, \theta} \|\hat{\epsilon}_t - \epsilon_t\|^2$ 

```

---



---

### Algorithm 2 Inference with VIN $\leftrightarrow$ DiT ensemble

---

**Require:** Forward schedule  $\alpha_t$ , Reverse Variance  $\sigma_t$

**Require:**  $N_s$  chunk size,  $N_{local}$  local size, Timesteps  $T$

Set  $x_T \sim \mathcal{N}(0, 1)$

**for**  $t = T - 1, \dots, 1$  **do**

$Z_t \leftarrow f_\alpha(X_t, t)$

**for**  $i = 0, \dots, \lfloor N/N_s \rfloor$  **do** ▷ Run in Parallel

$X_t^i \leftarrow X_t[:, iN_s : (i+1)N_s]$

$X_t^{local} \leftarrow X_t[:, iN_s - N_{local} : iN_s]$

$\hat{\epsilon}_t^i \leftarrow \epsilon_\theta(\text{concat}[X_t^{local}, X_t^i, Z_t], t)$

$\hat{\epsilon}_t^i \leftarrow \hat{\epsilon}_t^i[:, N_{local} + N_s]$

**end for**

**if** fuse tokens **then**  $\hat{\epsilon}^t = \text{TokenFusion}(\hat{\epsilon}^t)$

$\hat{\epsilon}_t = \text{concat}[\hat{\epsilon}_t^0, \dots, \hat{\epsilon}_t^{\lfloor N/N_s \rfloor}]$

$\mathbf{x}_{t-1} \leftarrow \frac{1}{\sqrt{\alpha_t}} \left( \mathbf{x}_t - \frac{1-\alpha_t}{\sqrt{1-\alpha_t}} \hat{\epsilon}_t \right) + \sigma_t \mathbf{z}$

**end for**

---

## 12. User Study Design

We set up a comparison of VIN against other state-of-the-art methods considered in this work. A cohort of humans was presented with two 256-frame videos at a time, generated from the same prompt, and asked to rate which video was better with an option to choose that they prefer them equally. One of the videos was always generated using our method and the order of the videos was randomized. Raters were asked to assess the videos on two metrics: (1) overall appearance and (2) temporal consistency. See Fig. 24 for a screenshot of the survey page. We presented the user with comparisons over 45 prompts. The prompt was selected at random from a pool of 25 prompts. The 45 comparisons were equally divided as nine comparisons against each of the five methods. Overall, we received 100 assessments, each between VIN and other methods. For each metric under consideration, we reported the percentage with which VIN was deemed better (wins), comparable (draws), and worse (losses).

## 13. Test Prompts

We detail the prompt suite used across evaluations performed in this work.

### 13.1. Prompts used for VBench Evaluation

- Subject Consistency:
  1. A giraffe running to join a herd of its kind
  2. A car turning a corner
  3. A car accelerating to gain speed
  4. A train accelerating to gain speed
  5. A cat drinking water
  6. A dog enjoying a peaceful walk
  7. An airplane soaring through a clear blue sky



Figure 21. Qualitative visualizations with and without global tokens. Frames, where identity begins distorting, have been highlighted with a red box.

- 8. A cow running to join a herd of its kind
- 9. An airplane landing smoothly on a runway

- 10. A motorcycle accelerating to gain speed
- 11. A truck turning a corner

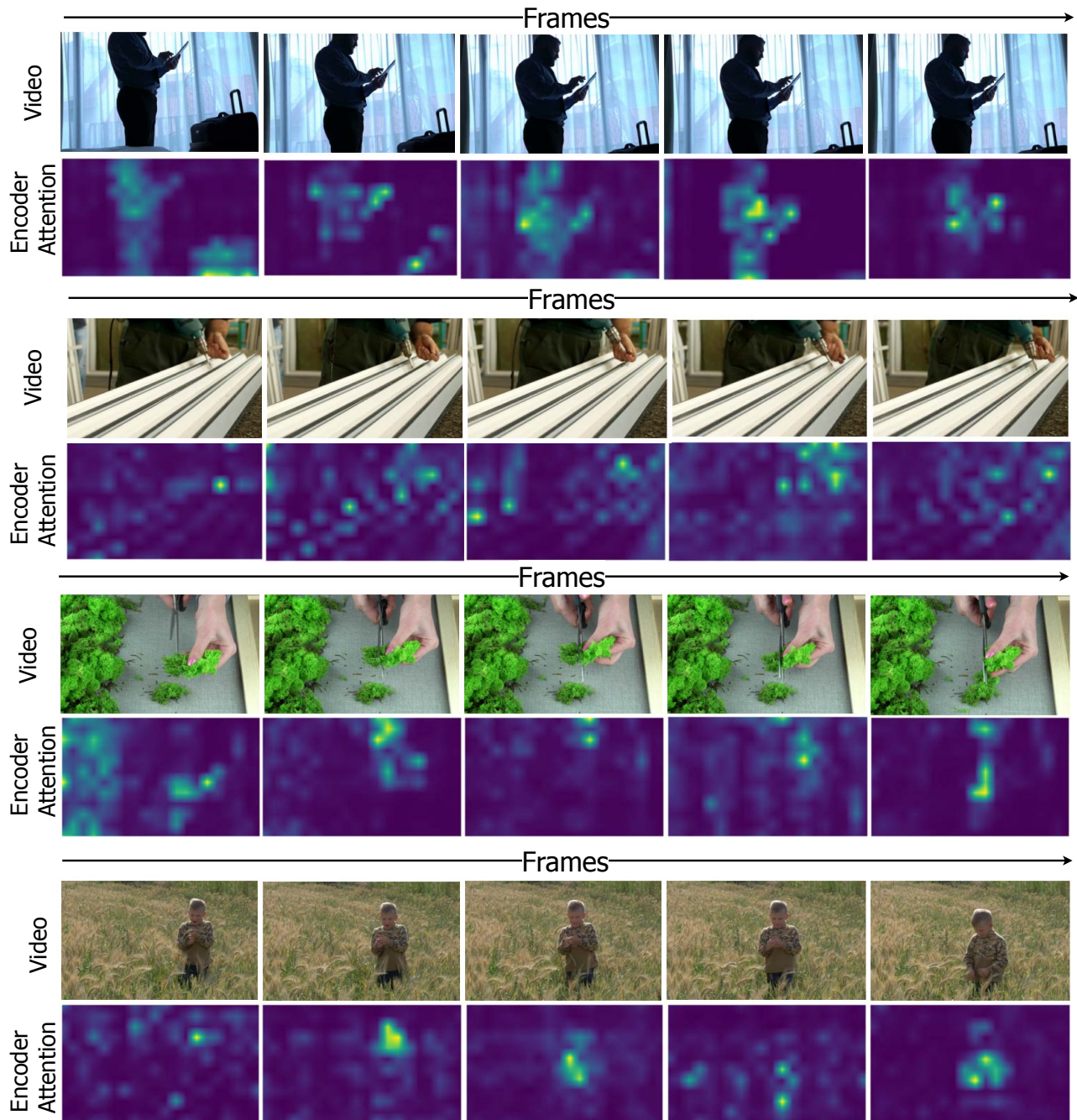


Figure 22. Qualitative visualizations across video and encoder attention. VIN exhibits motion-aware encoding, where it encodes dynamic objects as the video progresses.

- |  |  |
|--|--|
| 12. A giraffe bending down to drink water from a river | 18. A horse taking a peaceful walk                     |
| 13. A bicycle accelerating to gain speed               | 19. A cow chewing cud while resting in a tranquil barn |
| 14. A car stuck in traffic during rush hour            | 20. A dog running happily                              |
| 15. A truck stuck in traffic during rush hour          | 21. A person drinking coffee in a cafe                 |
| 16. An airplane accelerating to gain speed             | 22. A person walking in the snowstorm                  |
| 17. A cat playing in park                              | 23. A zebra bending down to drink water from a river   |

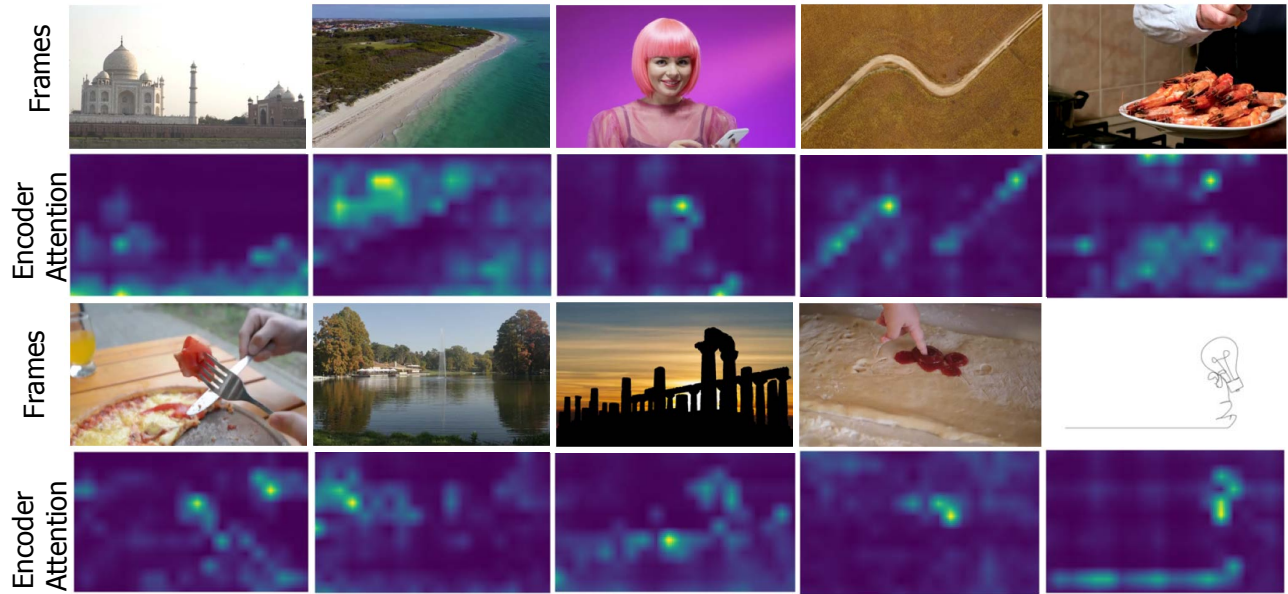
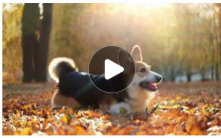


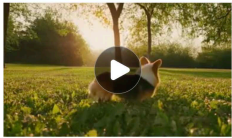
Figure 23. Qualitative visualizations across frames and encoder attention.

**Q XX: A cute happy Corgi playing in park, sunset, 4k**

Video 1



Video 2



---

Q xx: A cute happy Corgi playing in park, sunset, 4k

Video 1 looks better  
 Video 2 looks better  
 Both look equally good

---

Q xx: A cute happy Corgi playing in park, sunset, 4k

Video 1 has better consistency  
 Video 2 has better consistency  
 Both have equal consistency

Figure 24. User study design

- 24. A bicycle leaning against a tree
- 25. A cow bending down to drink water from a river
- Background Consistency:
  1. Underwater coral reef
  2. Phone booth

3. Hospital
4. Arch
5. Glacier
6. Jail cell
7. Sky
8. Highway
9. Classroom
10. Basement
11. Staircase
12. Bathroom
13. Volcano
14. Construction site
15. Valley
16. Beach
17. Ballroom
18. Fountain
19. Skyscraper
20. Raceway
21. Office
22. Ski slope
23. Golf course
24. Tower
25. Cliff
- Motion Smoothness
  1. A person washing the dishes
  2. A person giving a presentation to a room full of colleagues
  3. A sheep bending down to drink water from a river
  4. A horse taking a peaceful walk
  5. A bus stuck in traffic during rush hour

6. A bicycle accelerating to gain speed
  7. A car stuck in traffic during rush hour
  8. A truck turning a corner
  9. A dog drinking water
  10. A cat playing in park
  11. A motorcycle accelerating to gain speed
  12. A dog running happily
  13. A bird building a nest from twigs and leaves
  14. A person swimming in ocean
  15. A giraffe taking a peaceful walk
  16. A cow chewing cud while resting in a tranquil barn
  17. A person playing guitar
  18. A train crossing over a tall bridge
  19. A truck slowing down to stop
  20. A train speeding down the tracks
  21. A car turning a corner
  22. A zebra running to join a herd of its kind
  23. A bird soaring gracefully in the sky
  24. A motorcycle cruising along a coastal highway
  25. A truck accelerating to gain speed
- Temporal Flickering
    1. A tranquil tableau of a bunch of grapes
    2. A tranquil tableau of kitchen
    3. A tranquil tableau of palace
    4. A tranquil tableau in the heart of Plaka, the neoclassical architecture of the old city harmonizes with the ancient ruins
    5. In a still frame, parking lot
    6. A toilet, frozen in time
    7. In a still frame, a tranquil pond was fringed by weeping cherry trees, their blossoms drifting lazily onto the glassy surface
    8. A tranquil tableau of a chair
    9. A tranquil tableau of the jail cell was small and dimly lit, with cold, steel bars
    10. A tranquil tableau of an antique bowl
    11. A tranquil tableau at the edge of the Arabian Desert, the ancient city of Petra beckoned with its enigmatic rock-carved façades
    12. A laptop, frozen in time
    13. A tranquil tableau of a beautiful wrought-iron bench surrounded by blooming flowers
    14. A tranquil tableau of a wooden bench in the park
    15. In a still frame, in the vast desert, an oasis nestled among dunes featuring tall palm trees and an air of serenity
    16. A tranquil tableau of a bowl on the kitchen counter
    17. A tranquil tableau of a country estate's library featured elegant wooden shelves
    18. In a still frame, a tranquil Japanese tea ceremony room, with tatami mats, a delicate tea set, and a bonsai tree in the corner
    19. Indoor gymnasium, frozen in time
20. Static view on a desert scene with an oasis, palm trees, and a clear, calm pool of water
  21. A tranquil tableau of restaurant
  22. A tranquil tableau of a dining table
  23. A tranquil tableau of a tranquil lakeside cabin nestled among tall pines, its reflection mirrored perfectly in the calm water
  24. In a still frame, nestled in the Zen garden, a rustic tea-house featured tatami seating and a traditional charcoal brazier
  25. A tranquil tableau of barn
- Temporal Style
    1. A boat sailing leisurely along the Seine River with the Eiffel Tower in background, tilt down
    2. A boat sailing leisurely along the Seine River with the Eiffel Tower in background, zoom in
    3. A couple in formal evening wear going home get caught in a heavy downpour with umbrellas, tilt up
    4. A boat sailing leisurely along the Seine River with the Eiffel Tower in background, tilt up
    5. Snow rocky mountains peaks canyon. Snow blanketed rocky mountains surround and shadow deep canyons. The canyons twist and bend through the high elevated mountain peaks, with an intense shaking effect
    6. The bund Shanghai, in super slow motion
    7. A boat sailing leisurely along the Seine River with the Eiffel Tower in background, featuring a steady and smooth perspective
    8. The bund Shanghai, zoom in
    9. A couple in formal evening wear going home get caught in a heavy downpour with umbrellas, pan left
    10. A boat sailing leisurely along the Seine River with the Eiffel Tower in background, pan right
    11. A shark is swimming in the ocean, featuring a steady and smooth perspective
    12. A couple in formal evening wear going home get caught in a heavy downpour with umbrellas, zoom out
    13. A couple in formal evening wear going home get caught in a heavy downpour with umbrellas, with an intense shaking effect
    14. An astronaut flying in space, with an intense shaking effect
    15. An astronaut flying in space, in super slow motion
    16. A shark is swimming in the ocean, tilt up
    17. An astronaut flying in space, racking focus
    18. The bund Shanghai, pan right
    19. Gwen Stacy reading a book, tilt up
    20. The bund Shanghai, racking focus
    21. A shark is swimming in the ocean, pan right
    22. A cute happy Corgi playing in park, sunset, tilt up
    23. A cute happy Corgi playing in park, sunset, pan right
    24. A cute happy Corgi playing in park, sunset, featuring a steady and smooth perspective

25. A couple in formal evening wear going home get caught in a heavy downpour with umbrellas, in super slow motion
- Overall Consistency
  1. A beautiful coastal beach in spring, waves lapping on sand by Hokusai, in the style of Ukiyo
  2. A beautiful coastal beach in spring, waves lapping on sand by Vincent van Gogh
  3. A car moving slowly on an empty street, rainy evening
  4. A drone flying over a snowy forest
  5. A drone view of celebration with Christmas tree and fireworks, starry sky - background
  6. A panda playing on a swing set
  7. A panda standing on a surfboard in the ocean in sunset
  8. A space shuttle launching into orbit, with flames and smoke billowing out from the engines
  9. A teddy bear washing the dishes
  10. An artist brush painting on a canvas close up
  11. An astronaut feeding ducks on a sunny afternoon, reflection from the water
  12. An astronaut flying in space
  13. An ice cream is melting on the table
  14. An oil painting of a couple in formal evening wear going home get caught in a heavy downpour with umbrellas
  15. Few big purple plums rotating on the turntable. Water drops appear on the skin during rotation. Isolated on the white background. Close-up. Macro
  16. Golden fish swimming in the water
  17. Happy dog wearing a yellow turtleneck, studio, portrait, facing camera, dark background
  18. Motion colour drop in water, ink swirling in water, colourful ink in water, abstraction fancy dream cloud of ink
  19. Sewing machine, old sewing machine working
  20. Time lapse of sunrise on Mars
  21. Turtle swimming in ocean
  22. Two pandas discussing an academic paper
  23. Yellow flowers swinging in the wild
  24. Yoda playing guitar on the stage
10. Timelapse of sunrise on Mars
11. A giraffe running to join a herd of its kind
12. Cherry blossoms swinging by the ocean
13. Campfire at night in a snowy forest with starry sky in the background
14. A dog swimming
15. Beer pouring into a glass low-angle, wide shot
16. A raccoon wearing a suit playing the trumpet
17. A cat wearing sunglasses and working as a lifeguard at a pool
18. A fat rabbit wearing a purple robe walking through a fantasy landscape
19. Back view on young woman dressed in a yellow jacket walking in the forest
20. A shark swimming in clear Caribbean ocean
21. A petri dish with a bamboo forest growing within it that has tiny red pandas running around
22. A swarm of bees flying around their hive
23. A fantasy landscape
24. Aerial view of a snow-covered mountain
25. A dog wearing a Superhero outfit with red cape flying through the sky

### 13.2. Prompts used for User Study

1. A drone flying over a snowy forest
2. A panda standing on a surfboard
3. A teddy bear washing dishes
4. Happy dog wearing a yellow turtleneck, studio, portrait, facing camera, dark background
5. Golden fish swimming in the ocean
6. Yellow flowers swing in the wind
7. Two pandas discussing an academic paper
8. Smiling elderly gentlemen with rimmed glasses, tweed jacket, studio, standing still, burgundy background
9. Bear trying to learn calculus